HHS Public Access

Author manuscript

Mol Cell. Author manuscript; available in PMC 2024 April 01.

Published in final edited form as:

Mol Cell. 2023 June 01; 83(11): 1903–1920.e12. doi:10.1016/j.molcel.2023.05.008.

Irisin acts through its integrin receptor in a two-step process involving extracellular Hsp90α

Mu A[1,2], **Thomas E. Wales**[3], **Haixia Zhou**[4], **Sorin-Valeriu Draga-Coletă**[5,6], **Christoph Gorgulla**[1,7,8], **Katherine A. Blackmore**[1,2], **Melanie J. Mittenbühler**[1,2], **Caroline R. Kim**[1,2], **Dina Bogoslavski**[1,2], **Qiuyang Zhang**[1,2], **Zi-Fu Wang**[1,8], **Mark P. Jedrychowski**[1,2], **Hyuk-Soo Seo**[1,8], **Kijun Song**[1,8], **Andrew Z. Xu**[1,8], **Luke Sebastian**[1,8], **Steven P. Gygi**[2], **Haribabu Arthanari**[1,8], **Sirano Dhe-Paganon**[1,8], **Patrick R Griffin**[9,10], **John R. Engen**[3], **Bruce M. Spiegelman**[11,12]

[1]Department of Cancer Biology, Dana-Farber Cancer Institute, 360 Longwood Avenue, Boston, MA 02215, USA.

[2]Department of Cell Biology, Harvard Medical School, Boston, MA 02115, USA.

[3]Department of Chemistry and Chemical Biology, Northeastern University, 360 Huntington Avenue, Boston, MA 02115, USA.

[4]Department of Biological Chemistry and Molecular Pharmacology, Blavatnik Institute, Harvard Medical School, 240 Longwood Avenue, Boston, MA 02115, USA.

[5]Virtual Discovery, Inc 569 Hammond Street, Chestnut Hill, MA 02467, USA.

[6]Non-Governmental Research Organization Biologic, 14 Schitului Street, Bucharest 032044, Romania.

[7]Department of Physics, Harvard University, Cambridge, MA 02138, USA.

[8]Department of Biological Chemistry and Molecular Pharmacology, Harvard Medical School, 240 Longwood Avenue, Boston, MA 02115, USA.

[9]UF Scripps Biomedical Research, 130 Scripps Way, Jupiter, FL 33458, USA.

[10]Scripps Research, 130 Scripps Way, Jupiter, FL 33458, USA.

[11]Department of Cancer Biology, Dana-Farber Cancer Institute, 360 Longwood Avenue, Boston, MA 02215, USA.

[12]Department of Cell Biology, Harvard Medical School, Boston, MA 02115, USA.

Lead Contact: bruce_spiegelman@dfci.harvard.edu.

Author contributions

M.A performed and analyzed all the biochemical, biophysical and cellular experiments under the supervision of B.M.S.. T.E.W. performed and analyzed the HDX-MS experiments under the supervision of J.R.E.. P.R.G. helped to establish the HDX-MS assays. H.Z. performed negative-stain EM and cryo-EM. S.D. and C.G. generated the irisin-integrin docking model under the supervision of H.A.. K.A.B., M.J.M., C.R.K., D.B., Q.Z., Z.W., H.S., K.S., A.Z.X., L.S. and S.D. helped with the cellular, mice and biochemical experiments. M.P.J. performed the Mass Spectrometry experiments under the supervision of S.P.G.. M.A and B.M.S. cowrote the paper with the assistance from all other authors.

Declaration of interests

B.M.S. holds several issued patents on irisin. B.M.S. is an academic co-founder of Aevum Therapeutics, which is attempting to develop irisin as a therapeutic. M.A. is a consultant to Aevum Therapeutics.

Summary

Exercise benefits the human body in many ways. Irisin is secreted by muscle, increased with exercise, and conveys physiological benefits, including improved cognition and resistance to neurodegeneration. Irisin acts via αV integrins; however, a mechanistic understanding of how small polypeptides like irisin can signal through integrins is poorly understood. Using mass spectrometry and cryo-EM, we demonstrate that the extracellular heat-shock protein 90α (eHsp90α) is secreted by muscle with exercise and activates integrin αVβ5. This allows for high-affinity irisin binding and signaling through an Hsp90α/αV/β5 complex. By including hydrogen/deuterium exchange data, we generate and experimentally validate a 2.98 Å RMSD irisin/αVβ5 complex docking model. Irisin binds very tightly to an alternative interface on αVβ5 distinct from that used by known ligands. These data elucidate a non-canonical mechanism by which a small polypeptide hormone like irisin can function through an integrin receptor.

Keywords

Irisin; exercise; integrin; conformational states; extracellular Hsp90; integrin activation; fibronectin III domain; ligand binding; RGD motif; integrin signaling; HDX-MS; protein-protein docking

Introduction

Exercise benefits the body in many ways[1]. Our lab initially identified the protein PGC1α as a transcriptional coregulator of PPARγ and other nuclear receptors, which regulates mitochondrial biogenesis and adipose thermogenesis[2–5]. PGC1α is induced in the skeletal muscle of humans and rodents with exercise and it stimulates many important adaptations of muscle to exercise[6–10]. Muscle-selective PGC1α transgenic mice were then used as a platform for the discovery of muscle-secreted proteins regulated by PGC1α and exercise. These studies identified irisin, a cleaved and secreted product from a type-1 membrane protein FNDC5 (fibronectin-domain III (FNIII) containing 5), whose mRNA is increased upon forced PGC1α expression and exercise[11].

The amino acid sequence of irisin is 100% conserved between mouse and human. Irisin is a heavily glycosylated 12 kDa (112 aa) polypeptide structurally homologous to FNIII domain[11,12]. Measurement of the plasma levels of irisin using absolute quantification by tandem mass spectrometry reveals that irisin circulates at typical levels for polypeptide hormones (3–5 ng/ml range). Exercise elevates irisin circulating concentrations in both humans and mice[13–15]. Irisin mediates multiple metabolic effects including improving brain functions and resistance to neurodegeneration[16,17]. In bone, fat and hippocampus, irisin appears to function primarily via αV integrin receptors, particularly αVβ5. Since interactions between integrins and their typical large ligands, such as ECM proteins, are usually rather complex, how a small protein like irisin can interact with and function through an integrin receptor is not clear. Additionally, irisin has certain bioactivities, such as effects on cognition, not often associated with integrins.

Integrins are heterodimeric membrane receptors composed of noncovalently associated α and β subunits that bind extracellular matrix proteins, such as fibronectin, or counter receptors, such as I-CAM. In doing so, they mediate cell-matrix or cell-cell adhesion, respectively[18]. 18 α and 8 β subunits have been identified in vertebrates and these assemble into at least 24 known integrin heterodimers. These have different ligand specificities and signaling properties[18,19]. Integrins are composed of a large ectodomain responsible for extracellular ligand binding, a single-pass transmembrane domain and a short cytoplasmic tail[20]. Integrins populate an ensemble of at least three conformational states with different affinities for their ligands: low affinity-closed state, extended closed state, and a high-affinity open state[21].

On the surface of a resting cell, the energy landscape favors the closed state (>99%) and maintains only a very small fraction (~0.1%) of the integrins in the open confirmation[22–25]. Therefore, integrins need to be activated/opened for high-affinity extracellular ligand binding. The mechanism of integrin activation is complex, and the prevailing view highlights the reciprocal activation induced by both extracellular ligands that target the ectodomain head and intracellular ligands which targets the cytoplasmic tail[18,26]. Many well-studied integrin ligands like fibronectin exist at high concentrations in extracellular milieu (hundreds of microgram per ml in comparison to irisin that is at low nanogram per ml), and have relatively low affinities for their activated integrin receptors compared to other extracellular ligands. Although stimulatory/activating antibodies that target the ectodomain have been identified, endogenous extracellular factors that specifically mediate integrin activation, have not, to our knowledge, been discovered[27]. Importantly, the conformation and ligand-binding affinity of integrin can be affected by metal ions which bind integrin at the metal-ion dependent adhesion site (MIDAS)[28–30]. Of note, Mn^{2+}, through a rather unclear mechanism, largely shifts integrins to their open states and significantly improves ligand binding affinities of integrins in all conformational states[30].

αV integrins are one of the integrin families that lack the inserted αI domain and recognize the RGD motif – a conserved recognition sequence shared by many integrin ligands[31]. For most FNIII domain-containing integrin ligands, the RGD motif typically resides in a flexible loop that forms a small interface with both α and β integrin subunit heads at the RGD-binding site[29,32]. However, irisin is composed of a single FNIII domain without an RGD motif.

We have now identified an extracellular component for the interaction of irisin with its integrin receptor. Extracellular Hsp90α (eHsp90α) is an exercise-induced factor that mediates integrin activation via direct binding to the ectodomain of αVβ5. The αVβ5 receptor, activated by eHsp90α, has a very high affinity (K_d^{app} of ~30 nM) for irisin. Through biophysical and biochemical experiments, refined by multiple steps of MD simulations, we were able to generate and refine a docking model with 2.98 Å RMSD of the irisin/αVβ5 complex. This structure has important implications for integrin-small ligand dynamics, and how irisin mediates its physiological effects.

Results

eHsp90α is required for irisin binding to integrin αVβ5

To biochemically and biophysically characterize the interaction between irisin and integrin αVβ5, we expressed the ectodomain of this integrin and adapted the previously developed constructs for producing recombinant αVβ5 ectodomain. This integrin heterodimer was prepared as a C-terminally clasped, affinity tagged fusion protein from mammalian HEK293 cells (Figure 1A)[33]. The affinity-purified clasped αVβ5 was subsequently subjected to HRV3C protease cleavage, to generate the unclasped and untagged form (Figure 1A). Both subunits of the recombinant αVβ5 ectodomain are glycosylated with heterogeneous glycans, which can be removed by glycosidase treatment (Figures S1A and 1F). Wild-type, glycosylated recombinant irisin (His tagged or untagged) was produced from mammalian HEK293 cells as previously described (see Figure S1A and[14]).

Next, Bio-Layer Interferometry (BLI) was used to analyze the binding of irisin to αVβ5, and yielded an apparent dissociation constant (K_d^{app}) of 212 nM ± 53 nM (Figure 1B). To improve the purity of the recombinant αVβ5 ectodomain for structural analysis, we applied additional chromatographic steps and separated a “contaminating” protein which had a similar molecular mass (~90kDa) to the β5 subunit (Figure 1C). Notably, the binding affinity of irisin for this more highly purified αVβ5 was almost eliminated (Figure 1D). Of course, this result may be explained if one (or more) proteins that initially co-purified with the αVβ5 were necessary for high-affinity binding between irisin and αVβ5. Using mass spectrometry, we identified a major protein associated with the initial αVβ5 preparations as Hsp90α (Figures 1C and S1B).

To determine whether Hsp90α alone binds αVβ5 directly, recombinant human Hsp90α was purified from *E.coli* and was used in a biochemical pull-down experiment. Clasped αVβ5 or control peptide containing only the tagged dimerization motifs was immobilized and incubated with an equal molar concentration of Hsp90α. The Hsp90α co-precipitated with αVβ5, but not with the control peptide (Figure S1C). We then forced the maximal stoichiometry of the αVβ5/Hsp90α complex by adding 20-fold molar excess of Hsp90α, followed by extensive washing steps to remove the unbound Hsp90α. The αVβ5 and its bound Hsp90α were eluted off the beads by HRV3C protease cleavage. The reconstituted αVβ5/Hsp90α eluted as a stable high-mass particle by gel filtration chromatography, compared to αVβ5 alone (Figure 1E). The peak fractions of αVβ5/Hsp90α and αVβ5 alone were deglycosylated, and quantification of the protein bands in the complex peak fraction revealed an Hsp90α:αV:β5 ratio of ~1:1:1 (Figure 1F).

These data suggest that Hsp90α might facilitate the interaction between irisin and αVβ5. To measure the binding affinity in solution, we used the polarization of fluorescently labeled irisin (A488-irisin) to examine its binding to either αVβ5 or the αVβ5/Hsp90α complex. In contrast to αVβ5 alone, which showed a very low affinity for irisin, the αVβ5/Hsp90α complex binds irisin with much higher affinity (K_d^{app} of 31 nM ± 4 nM) (Figure 1G). To determine whether the A488 label or the His tag (fused to irisin) contributed to the binding, we used competition assays in which fixed concentrations of A488-irisin and αVβ5/Hsp90α were mixed with varying concentrations of unlabeled His-tagged irisin (irisin-His), or

unlabeled and untagged irisin. Irisin-His and untagged irisin showed similar affinity for the αVβ5/Hsp90α complex, with K_d^{app} of 52 nM and 50 nM, respectively (Figure 1H). Taken together, Hsp90α was identified as an extracellular factor from cultured mammalian cells that mediates irisin/αVβ5 interaction by associating directly with αVβ5.

eHsp90α level is increased with exercise in muscle interstitial fluid and in plasma

Hsp90α does not contain an N-terminal signal sequence, and is released from cells through an unconventional secretion mechanism[34,35]. eHsp90α binds a number of cell surface receptors, and modulates their downstream signaling pathways through as yet unidentified mechanisms[36–41]. Since irisin levels increase with exercise[13–15], we evaluated eHsp90α levels in response to a single, intense bout of exercise in mice. To harvest the interstitial fluids (IF) of muscle, we adapted a technique that was used previously for analyzing metabolites of the gastrocnemius muscle (Figure 2A and[42–45]). We found that levels of eHsp90α protein in the IF samples were elevated with exercise, while the total levels of Hsp90α protein within muscle tissue remained unchanged (Figures 2B and C). Interestingly, eHsp90α protein levels were also upregulated in plasma taken from mice that had rested for different amounts of time post-exercise (Figure 2D). This is in contrast to another extracellular heat shock chaperone protein, HspA14, whose levels remain constant before and after exercise (Figure 2E).

To ensure that the elevation of eHsp90α in IF is a specific, exercise-mediated regulatory process, rather than a nonspecific release of cellular content from damaged cells, we analyzed the acute exercise-induced muscle-specific extracellular proteome dataset[46] and found that only 4 (one Hsp70 isoform and three Hsp90 isoforms) out of 22 identified chaperone proteins, including Hsp90α (encoded by Hspaa1), were significantly upregulated (significant if FDR <0.05) in the IF of the exercised mice compared to the sedentary group (Figure 2F).

eHsp90α is required for optimal cellular actions of irisin

We then tested the role of Hsp90α in the binding of irisin to αVβ5 in live cells, along with certain irisin-mediated cellular effects. Cultured HEK293T cells, with or without forced expression of integrin αV and β5 subunits, were used in gain-of-function experiments, as previously described[14], and to assess irisin binding to the transfected cells using A488-irisin. Cellular bioactivity of the fluorescently labeled irisin was validated by treating HEK293T cells transfected with control plasmid or full-length αV and β5 plasmids with unlabeled irisin, fluorophore A488 alone, or A488-irisin. Irisin-induced integrin signaling was tested by probing the canonical FAK phosphorylation, as shown previously[14]. A488-irisin plus unlabeled irisin (but not A488 alone) induced similar integrin signaling in cells that ectopically expressed αV and β5 subunits (Figure S2A). Irisin binding was also examined in live cells by tracing A488 fluorescence using confocal microscopy; A488-irisin binding was detected in cells that expressed αVβ5 ectopically, but not in the cells transfected with control plasmid. Importantly, this binding was significantly enhanced in cells that were pretreated with recombinant Hsp90α (Figures 3A and S2G). This same cellular system was then used to investigate integrin signaling. These data confirmed that irisin treatment induced little integrin signaling in control HEK293T cells, but cells

that ectopically expressed αVβ5 showed irisin-induced phosphorylation of FAK in a dose-dependent manner (Figure 3B). Of note, pretreatment with recombinant Hsp90α shifted the dose response leftwards. A maximum pFAK signal was induced by 1.0 nM irisin in cells not receiving Hsp90α, but 0.1 nM was sufficient to stimulate a maximum signal in cells with added external Hsp90α (Figure 3B). Interestingly, Hsp90α induced low levels of pFAK in the absence of αVβ5, suggesting a role of Hsp90α in other integrin-mediated signaling. To investigate if other chaperon proteins function in the similar manner, we tested Hsp70, as the level of one Hsp70 isoform (Hspa5) was also elevated in muscle extracellular fluid samples with exercise (Figure 2F). A direct interaction between Hsp70 and αVβ5 was not detected in the pull-down assay (Figure S2B), and no further improvement of irisin-mediated integrin signaling was observed in HEK293 cells ectopically expressing αVβ5 (Figure S2C).

eHsp90α is present on the surface of many cell types, and mediates specific cellular functions, such as melanoma migration[47–50]. αV integrins are expressed in many melanoma cell lines, and αVβ5 is on the surface of a variety of melanoma cells that are highly metastatic[51]. However, the relation between eHsp90α and αVβ5, as well as their molecular functions in melanoma cells, has not been previously addressed. We chose human melanoma cells (SK-Mel2) to explore the role of the endogenous eHsp90α in irisin binding and irisin-mediated cellular effects. Immunofluorescent staining was used to confirm the expression of cell surface eHsp90α on SK-Mel2 cells. Live cells were chilled on ice and incubated with Hsp90α antibody to visualize the Hsp90α on the plasma membrane. Cell surface eHsp90α was detected on more than 70% of the cells (Figures 3C and D). The cellular interaction between eHsp90α and integrin αVβ5 on the cell surface was next examined using co-immunoprecipitation. Both αV and β5 subunits co-immunoprecipitated with cell surface eHsp90α (Figure 2G), indicating the assembly of endogenous αVβ5/Hsp90α complex in melanoma cells. Next, to examine the binding of irisin to SK-Mel2 cells, A647-irisin, instead of A488-irisin, was used to avoid the high background signal generated by melanoma cellular autofluorescence. More than 80% of the SK-Mel2 cells pretreated with a control antibody showed irisin binding, and pre-treatment with anti-Hsp90α antibody significantly reduced the number of A647-irisin-positive cells to ~10% (Figures 3E and F). Finally, we assessed the viability of SK-Mel2 cells in response to irisin treatment. Crystal violet staining revealed a dose-dependent irisin-mediated reduction in cell viability; treatment with 30~100 ng/mL irisin led to 10~40% reduction of the cell viability, respectively. Importantly, this reduction of viability could be inhibited by pre-treatment with an Hsp90α antibody but not with a control antibody (Figures 3G and H).

To test the role of eHsp90α *in vivo*, we injected Hsp90 antibody subcutaneously 24 hrs before a bolus injection of recombinant irisin directly into the inguinal fat pads (iWAT) of mice. iWAT was harvested 20 min after irisin injection for probing integrin signaling and 45 min after irisin injection for measurement of thermogenic gene expression. The irisin-induced phosphorylation of FAK, CREB and Src and upregulation of UCP1, Cidea and Dio2 (as shown previously in[14]) were strongly reduced by administration of the anti-Hsp90 antibody (Figures 3J and S2D). In cultured melanoma cells, endogenous eHsp90α associates with αVβ5 allowing for irisin actions (Figures 3C–3I). To investigate the formation of αVβ5/eHsp90α complex *in vivo* under physiological conditions, we again adopted the acute exercise protocol to elevate the plasma level of eHsp90α, and probed αVβ5/eHsp90α

complex in iWAT. This tissue was previously shown to express αVβ5 integrin[14]. As shown in Figure S2E, the αV subunit was effectively immunoprecipitated from iWAT lysates using anti-αV antibody. A significant but fairly small percentage (<1%) of total Hsp90α was co-precipitated with αV in the iWAT of the exercised mice, while the levels of co-precipitated Hsp90α in the sedentary mice were barely detectable under these conditions.

Taken together, these data indicate a role of exogenous and endogenous Hsp90α in irisin actions both in cultured cells and *in vivo*.

Hsp90α activates αVβ5 for irisin binding

αV integrins prefer to stay in the low energy "closed" state, a state that is generally considered to be non-permissive for ligand binding. These integrins needs to be activated to achieve high ligand-binding affinity, allowing efficient RGD-mediated integrin signaling[52]. In theory, Hsp90α could facilitate the interaction between irisin and αVβ5 either by activating or stabilizing αVβ5 into its high-affinity state, or by associating with αVβ5 to provide additional sites for irisin binding, or both. To investigate the molecular mechanism underlying the role of Hsp90α in mediating the irisin/αVβ5 interaction, cryogenic electronic microscopy (cryo-EM) was used to study the conformation of the individual αVβ5 particles in the presence or absence of Hsp90α. We first looked at Hsp90α alone using negative staining EM, and observed a large population of particles which are significantly smaller and more heterogeneous than the previously revealed Hsp90α dimer particles under EM[53]. The observed structural changes were most likely introduced during EM grid preparation. To avoid this apparently non-native heterogeneity, we first treated the samples with chemical cross-linking. This succeeded and we saw a preponderance of two states: an "extended" (Apo or ADP-bound state) and a "fastened" (ATP bound) states of the Hsp90α (Figures S3A and S3B)[53].

Next, we sought to determine how Hsp90α affects the conformational states of αVβ5. The αVβ5 and αVβ5/Hsp90α samples for cryo-EM were prepared without using cross-linker so that native αVβ5 particles were picked up during particle selection. We adopted both "template-free" (method 1) and "template-directed" (method 2 and 3) methods to pick particles for analysis (see methods). Briefly, for unbiased "template-free" method, we used random blob picker to select particles for 2D classification, and the generated 2D classes were further analyzed based on the previously described ensembles of three distinct confirmations: closed (low affinity state), extended closed and open (high affinity state)[21]; for "template-directed" methods, six 2D classes containing "closed", "extended closed" and "open" states were first generated from either αVβ5 or αVβ5/Hsp90α samples using blob picking, and the generated 2D classes were subsequently used as the templates to pick particles from the αVβ5 and αVβ5/Hsp90α micrographs (Figures 4A and B). The number and percentage of particles generated in each state were quantified for both αVβ5 and αVβ5/Hsp90α samples, with or without particles classified into a "likely open" group included. Analyzed by all three different methods, we saw more "open" and fewer "closed" αVβ5 particles in the αVβ5/Hsp90α compared to the αVβ5 alone sample, suggesting that Hsp90α functions to "open" αVβ5 for tight irisin binding (Figures 4B, C and S3C). This result is similar to the measured effects of certain exogenous antibodies which bind integrin

extracellular domains and activate the receptors from a low- to a high-affinity state for ligand binding[54–56],

We next examined whether Hsp90α affects the affinity of irisin for αVβ5. To do this, we took advantage of another method, Mn^{2+} ion supplementation, well known to chemically activate a variety of integrins[30,57,58]. αVβ5 was activated either by adding Mn^{2+} ion, or by forming a complex with Hsp90α (see Figures 1F and 1G), and the affinity of αVβ5/Mn^{2+} and αVβ5/Hsp90α for A488-irisin was compared using fluorescence anisotropy. In contrast to αVβ5 alone in Mg^{2+}/Ca^{2+} buffers, the binding affinities of αVβ5/Mn^{2+} and αVβ5/Hsp90α for irisin were very similar, with the K_d^{app} of 28 nM ± 4 nM and 37 nM ± 7 nM, respectively (Figure 4D). Furthermore, the presence of both Hsp90α and Mn^{2+} did not further improve the affinity of αVβ5 for irisin (Figure S3D). These results strongly suggest that the main function of Hsp90α is to activate or stabilize αVβ5 in the open structure to allow ligand binding. Importantly, once this integrin structure is "opened", Hsp90α does not appear to further improve the affinity of the receptor for irisin (Figure 4E).

Intracellular Hsp90α is an ATP-dependent chaperone. We therefore investigated whether the ATPase activity of Hsp90α is essential for mediating the irisin-αVβ5 interaction. After stripping off the originally bound nucleotide on Hsp90α, we recharged it with various nucleotides (see methods). Subsequently, the binding between αVβ5 and recombinant Hsp90α was investigated in different nucleotide states: Apo, ATP, nonhydrolyzable ATP (AMP-PNP) or ADP. Using a pull-down assay, we detected that, regardless of the nucleotide state, a similar amount of Hsp90α co-precipitated with αVβ5 (Figure 4F). A similar approach was used to test the function of an ATPase-deficient Hsp90α mutant G95D[59]. As shown in Fig 4G, this mutant bound αVβ5 with a similar affinity to the wild-type Hsp90α (Figure 4G). This suggests that the classic chaperone activity of Hsp90α, depending on ATP, is not required for the Hsp90α-αVβ5 interaction.

Biophysical characterization of the irisin/αVβ5 complex suggests an unconventional ligand-integrin interaction

Irisin differs in several ways from other integrin ligands: first, as a small polypeptide hormone ligand, irisin contains only one distinguished functional domain that shares limited sequence homology (15~20% identity), but great structural homology, to fibronectin III domains (Figure S4A). Furthermore, it does not contain an RGD motif that is considered to be the hallmark of integrin ligands (Figure S4A). Moreover, irisin plasma level is much lower compared to many known integrin ligands. While these results argue that eHsp90α serves as a physiological pathway to activate integrin, mediating both irisin binding and signaling, the exact mode of activation of integrins by irisin would require understanding at the atomic level.

To generate a structural model of the irisin-αVβ5 complex, we first estimated the binding stoichiometry between irisin and αVβ5, using a form of the classic Job plot where the concentration is held constant and mole fraction is varied. In this case, we detected the binding by MicroScale Thermophoresis (MST)[60]. Briefly, the MST response is plotted against the mole fraction of the ligand, and the maximum amount of complex formation (minimum response in the MST measurement) occurs at the mole fraction that corresponds

to the complex composition. Two linear fitting curves intersected at ~50% mole fraction of irisin (see Figure 5A), suggesting that one irisin molecule binds to one αVβ5 heterodimer. The binding stoichiometry suggested that the irisin used here, expressed in mammalian cells (irisin-mam), is a monomer. This is quite distinct from the previously characterized dimeric form of irisin that was produced in bacteria (irisin-bac)[12]. Irisin-mam is heavily glycosylated and appears to be much larger than its protein molecular mass (~14 kDa) in SDS-PAGE (Figure S1A). To determine the oligomeric state of irisin-mam, we used SEC-MALS to measure the absolute molar mass of irisin protein and its conjugated glycans. Irisin eluted as monodispersed particles by size exclusion chromatography with an average molecular mass of 27.3 kDa, as detected by light scattering. We further performed conjugate analysis and determined the irisin protein mass of 16.7 kDa plus the glycan mass of 10.8 kDa. These data indicate that irisin-mam is a monomer in solution (Figure 5B).

To characterize the effects of binding between irisin and αVβ5, we used hydrogen/deuterium exchange mass spectrometry (HDX-MS). We did this with large amounts of highly purified recombinant αVβ5 ectodomain in the presence of Mn^{2+} which permitted much more robust HDX than our previous HDX/MS work[14]. The use of Mn^{2+} instead of eHsp90α to "open" the integrin simplified the HDX/MS analysis of irisin binding to αVβ5. Regions of αVβ5 were found protected in the complex (Figure 5C and Data S1). Of note, the sites that are protected by irisin are mostly on the β5 subunit (Figure 5D), and most of the sites are distinct from the RGD binding sites mapped in other αV integrins by HDX[61]. The loop of the β propeller domain of the αV subunit containing the Mn^{2+} binding site close to the thigh domain was strongly protected from HDX in the complex, indicating that irisin binding further stabilized αVβ5 in the extended open confirmation[32]. Little change in HDX signal was observed within irisin itself, indicating that conformational rearrangements or changes to conformational dynamics did not occur in irisin as a result of binding to this integrin.

Atomic resolution model of the irisin/αVβ5 complex

Finally, we generated a docking model of the irisin/αVβ5 complex, refined by multiple steps of MD simulation[62]. The experimental results of binding stoichiometry, as well as the HDX-MS results were incorporated as restraints during the docking process (Figure 6A and Data S2). Notably, this model revealed an extensive binding interface, burying 1586 $Å^2$ of irisin that involves five of its six inter-strand loops and four of its seven β-sheets. On the integrin side, most of the binding interface is on the βI domain in the β5 head, and only three loops of the β propeller domain in the αV head right at the α/β subunit interface are involved. Complete exposure of the irisin binding site requires αVβ5 to be in the "open" state (Figure 6B and Data S3). This is in striking contrast to the binding of FN10 to its integrin receptors in which their contact area is only a few hundreds of $Å^2$ and is solely contributed by the RGD loop of FN10 (Figure 6C). The binding of irisin to integrin is dominated by electrostatic interactions, where one acidic patch and one basic patch on irisin well fit into the corresponding basic and acidic grooves on αVβ5 (Figure 6D). Interestingly, the amino acid residues that interact with irisin are not assembled into the structural grooves on αVβ5 adopting the closed confirmation, suggesting that irisin binding requires αVβ5 to be in the open state.

Several residues at the irisin/αVβ5 interface stabilize the intermolecular interactions by bonding with more than one residue. For example, E991 in the β5 subunit and E82 in the αV subunit within the acidic groove binds H13, S22, S58, and R44, Q39 in irisin, respectively; R905 and K923 sitting in the basic groove of β5 subunit interact with Q50, E51, V52, and V31, T54 in irisin, respectively (Figure 6E). Given that the N- and C-termini of irisin align with those of integrin in the same direction, it is unlikely that FNDC5, as a membrane protein, can serve as a "counter receptor" of integrin. Although irisin is a small polypeptide integrin ligand, this unusually large interface likely gives rise to the high-affinity integrin binding.

Besides the difference in the size of the binding interface which likely accounts for the different binding affinity, we also compared the actual integrin binding sites between irisin and the fibronectin FN10 domain. FN10-αVβ3 complex structure (PDB 4MMX) was used for fibronectin alignment to dock FN10 onto αVβ5. Distinct from the canonical RGD-mediated integrin ligand binding site, irisin binds to the opposite side of αVβ5 (Figure 6C).

Lastly, the irisin-αVβ5 interface in the model is largely overlapping with the irisin dimer interface shown in a crystal structure of bac-irisin[12]. This data predicts a significantly lower affinity of the bacterial irisin as a dimer compared to the higher affinity of mammalian irisin monomer for αVβ5.

Validation of the irisin/αVβ5 complex model

This model of the irisin/αVβ5 complex is surprising for at least two reasons. First, the irisin binding site on αVβ5 is completely distinct from the binding sites for other FNIII domain-containing ligands. Hence, they should not be competitive with irisin for binding to αVβ5. Second, the large irisin-αVβ5 interface in this model likely accounts for the high affinity binding of the irisin monomer, rather than the dimer, to αVβ5. This is because the irisin-αVβ5 interface largely overlaps with the irisin dimer interface, so that the αVβ5 binding site on irisin could be masked by the other irisin subunit in the irisin dimer. Therefore, αVβ5 would sterically compete with one irisin subunit in the dimer for binding to the other irisin monomer, resulting in apparently low affinity of irisin dimer for αVβ5. To examine these predictions, we first compared the binding of irisin to αVβ5 with that of a classical FNIII-domain integrin ligand. Irisin shares structural homology with the fibronectin FNIII 10th domain (FN10)[12], but lacks an RGD that is present in this and many other FNIII domain-containing αVβ5 ligands (Figure S4A). We prepared a 10 kDa protein containing just the FN10 domain of fibronectin and tested the affinity between FN10 and αVβ5 using the fluorescence anisotropy binding assay with A488-labeled FN10. This yielded a K_d^{app} of 146 nM ± 23 nM for the FN10 protein, almost 5-fold weaker than the affinity between irisin and αVβ5 (Figure 7A). To determine experimentally whether irisin binds αVβ5 at a different site from that occupied by the canonical RGD-mediated integrin binding adopted by FN10, a fluorescence anisotropy competition assay was used. This employed fixed concentrations of A488-FN10 and αVβ5, and varying amounts of either unlabeled irisin or FN10. While unlabeled FN10 binds αVβ5 competitively with a K_d^{app} of 239 nM, the unlabeled irisin did not show any detectable competition with FN10. This

indicates that these two FNIII domain containing proteins, irisin and FN10, do not compete for binding at the same integrin site, and the presence of irisin at indicated concentrations did not affect FN10/αVβ5 complex stability (Figure 7B). To further emphasize this point, we asked whether a single αVβ5 could bind irisin and the FN10 protein simultaneously. A Fluorescence Resonance Energy Transfer (FRET) assay was performed using A488-FN10 and A555-irisin, and significant FRET was detected only in the presence of αVβ5. These data indicate that the fibronectin FN10 and irisin can bind αVβ5 simultaneously and in close proximity (Figure 7C).

Next, we examined whether the irisin monomer has higher affinity for αVβ5 compared to irisin dimer. As shown in Figure 5B and[12], irisin-mam is a glycosylated monomer and irisin-bac is a non-glycosylated dimer. We compared the affinities of αVβ5 for irisin-mam and irisin-bac. The latter binds αVβ5 with a K_d^{app} of 256 nM ± 14 nM, about 8-fold weaker than that for irisin-mam, when measured by the fluorescence anisotropy binding assay with A488-irisin-bac (Figure 7D). To examine whether αVβ5 sterically competes with one of the irisin subunits in the dimer to bind the other irisin monomer, we then investigated whether irisin-mam competes with irisin-bac for the same binding site on αVβ5. We used fluorescence anisotropy in a competition assay with fixed concentrations of A488-irisin-bac and αVβ5, and varying amounts of unlabeled irisin-bac or irisin-mam, which yielded a K_d^{app} of 294 nM and 35 nM, respectively. It is noteworthy that both unlabeled irisin-bac and irisin-mam achieved 100% inhibition at higher concentrations, indicating that they both bind αVβ5 at the same site (Figure 7E). Lastly, we generated the non-glycosylated irisin monomer mutant R75E from bacteria as previously described[12], and performed the same anisotropy competition assay as Figure 7E. The monomeric mutant binds αVβ5 with similarly high affinity (K_d^{app} of 42 nM) as irisin-mam, compared to the wild type irisin bacterial dimer (K_d^{app} of 299 nM), and 100% inhibition was achieved at the micromolar concentration range of both forms of irisin (Figure 7F). Collectively, these data provide validation of key aspects of this model ofirisin-αVβ5 binding.

Finally, we generated two αVβ5 mutants by reversing the charge of the amino acid residues that mediate irisin interaction and reside in the center of the basic (R218E) and acidic (E304R) grooves, respectively. The mutants showed ~80% (E304R) and > 90% (R218E) reduction of their affinities for irisin compared to WT (Figure 7G).

Discussion

Irisin is a muscle-derived polypeptide hormone whose levels increase with exercise in rodents and humans[13–15]. Multiple studies in rodents, both gain and loss of function, indicate that irisin represents a potentially critical link between exercise and adaptations of the body to exercise. In light of this, a more comprehensive knowledge of ligand-receptor dynamics should be particularly useful to obtain an understanding of irisin-mediated effects and could inform the development of irisin-based therapeutics.

In this paper, we show that irisin employs an alternative two-step process, involving another extracellular protein Hsp90α in integrin activation. Given the broad tissue expression of Hsp90α, it seems very likely that eHsp90α may participate in other integrin-mediated

cellular events. In addition, identifying eHsp90α as a stress-induced factor used by irisin to mediate its signaling, suggests that irisin may have important functions in other stress-induced pathological conditions.

Our docking model, based on the demonstrated biochemical data and biophysical HDX-MS data, revealed a distinct integrin-ligand binding site. Interestingly, this model illustrates a broader, “pancake-like” positioning of irisin mainly on the β5 subunit, quite distinct from the known RGD binding site. The multiple atomic interactions in this conformation provide for high affinity and importantly, are also capable of inducing a global conformational rearrangement of the integrin subunits to elicit signal transduction. Of course, how this signaling in the end differs from that generated by RGD-containing ligands remains to be determined.

Glycosylation has important roles in protein solubility, stability, structure, secretion and other cellular functions. Previous elegant work by Schumacher et al (2013) clearly showed that unglycosylated irisin produced in bacteria exists as a homodimer, both in solution and in a crystal structure[12]. In contrast, we show here that irisin produced from HEK293 cells is a highly glycosylated monomer that nevertheless binds integrin with high affinity. In contrast, the bacterially-produced irisin, which is a dimer, binds integrin much more weakly. Interestingly, one of the predicted irisin glycosylation sites resides close to the dimer interface, suggesting that irisin glycosylation might affect its state of oligomerization, thus affecting irisin’s affinity for integrin. Of course, another consideration going forward is that the glycosylation profile of any recombinant protein might be influenced by the repertoire of glycosylation enzymes and transporters expressed by any particular host “producer” cell[63–65]. For instance, more sites were shown to be glycosylated extensively in recombinant proteins produced in HEK293 cells compared to those produced in CHO cells, and the composition and the shape of the glycans are also markedly different[63–65].

Irisin appears to readily pass the blood brain barrier (BBB) to affect several critical brain functions, notably learning and memory in two Alzheimers disease models[16], as well as a model of Parkinson’s Disease caused by α-synuclein injection[17]. In addition, genetic ablation of FNDC5 renders mice less able to gain the cognitive benefits of exercise. It is therefore noteworthy that αV integrins are abundantly expressed on the brain endothelial cells, pericytes and astrocytes that constitute the BBB. Thus, the receptor dynamics described here may be used by irisin for receptor-mediated transcytosis[66,67] and for this myokine to cross the BBB. Taken together, these studies provide information that may direct the design of new forms of irisin with improved activity and/or improved pharmacological kinetics.

Limitations of the study

We identified eHsp90α as one key factor to assist irisin in mediating its actions through an integrin receptor. However, different stimuli may induce alternative factors to achieve a similar two-step process in different cell types and tissues. Further investigation in other irisin-responsive systems, such as α-synuclein-induced cortical neurons, is required for exploring other potential mechanisms. In addition, how Hsp90α interacts with integrin to open it up has not yet been fully addressed here, and HDX/MS analysis as well

as binding test using individual domains of Hsp90α and integrin would provide more detailed information. Finally, although the irisin/αVβ5 structural model has been validated biochemically, it may be important to note that further validation in cultured cells and in vivo in mouse models could be done in the future to help dissect downstream pathways elicited by irisin in comparison with those induced by canonical integrin ligands.

STAR METHODS:

RESOURCE AVAILABILITY

Lead contact—Further information and requests for the resources and reagents should be directed to and will be fulfilled by the Lead Contact, Bruce Spiegelman (bruce_spiegelman@dfci.harvard.edu).

Materials availability—Unique material generated in this study, such as fluorescent irisin, will be available from the Lead Contact upon request.

Data and code availability

- All data, including mass spectrometry proteomics data and unprocessed and uncompressed images, from this publication have been deposited and are publicly available as the date of publication. Accession numbers and DOI are listed in the key resources table.
- This paper does not report original code.
- Any additional information required to reanalyze the data reported in this paper is available from the Lead Contact upon request.

EXPERIMENTAL MODEL AND SUBJECT DETAILS

Mice—Mice used for this study were housed at 22 °C, unless stated differently. They were housed with a 12h light/dark cycle and had unlimited access to food and water. Wild-type, 8 week old, male mice for exercise experiments were obtained from The Jackson Laboratory (C57BL/6J, #000664). All procedures were performed according to the NIH Guide for the Care and Use of Experimental Animal and approved Institutional Animal Care and Use Committee of Beth Israel Deaconess Medical Center.

Cell culture—Expi293F cells were purchased from Life Technologies (A14527) and maintained in Expi293 medium (Life Technologies A1435101) at 37 °C shaking incubator with 8% CO_2 at 100 rpm. HEK293T cells were purchased from ATCC (CRL-3216) and maintained in growth medium DMEM supplemented with 10% fetal bovine serum and penicillin/streptomycin at 37 °C. SK-Mel-2 cells were purchased from ATCC (HTB-68) and maintained in growth medium DMEM supplemented with 10% fetal bovine serum and penicillin/streptomycin at 37 °C.

METHOD DETAILS

Acute exercise protocol—Mice were trained on a motorized treadmill (Columbus Instruments) for three consecutive days. The exercise protocol was adapted from Reddy

et al. with minor modifications[45]. In brief, mice were trained 5 min at 12 m/min followed by a 1 min rest. Subsequently, mice run another 5 min at 12 m/min and 5 min at 14 m/min. On the third day of training, sedentary mice were removed from the treadmill and exercise mice were kept running for a total of 45 min with ramped up speed of 2 m/min every 5 mins and maximum speed of 26 m/min. Mice were sacrificed either 0 h, 30 min, 60 min, 2 h, or 4 h after the run, as indicated. Blood samples were taken, the gastrocnemius muscle was dissected and IF was isolated. Blood was allowed to clot for 15 min at room temperature, and centrifuged 10 min at 10,000 × g to remove the clot. Tissue, IF, and serum samples were used for western blot analysis using an α isoform specific anti-Hsp90 antibody (Invitrogen PA3–013). IF isolated 60 min post exercise was used for proteomic analysis. For immunoprecipitation assay, mice were sacrificed 60 min after the run and both inguinal fat pads were taken.

Interstitial fluid isolation—Rapid IF isolation was modified from previous procedures[42–45]. Briefly, gastrocnemius muscle was dissected, placed into a 20 μm nylon mesh (Millipore Sigma NY2004700), and fixed in a 1.5 ml tube. Subsequently, tissue was centrifuged at low speed (600–800 × g) for 10 min at 4 °C. IF was snap frozen and kept at −80 °C for further processing and analysis.

Immunodepletion of IF and Serum—Serum and IF samples were immunodepleted using R&D Systems™ Proteome Purify 2 Mouse Serum Protein Immunodepletion Resin (R&D Systems MIDR002020). The protocol was performed as described by the manufacturer. Briefly, 10 μl IF or serum was mixed with 1 ml of the immunodepletion resin and incubated on a rotator shaker at room temperature for 45 min. Subsequently 1 ml of resin was equally split into two SpinX filter tubes (R&D Systems SPINX8160036) and centrifuged at 1,500 g for 2 min. Flowthrough was collected, protein concentration was analyzed using Micro BCA™ Protein Assay Kit (Thermo Scientific 23235), and samples were snap frozen and kept at −80°C for further analysis.

Protein in-gel digestion, peptide isobaric labeling, LC-MS/MS analysis and mass spectrometry data processing—Silver-stained gel bands were excised, destained with acetonitrile, and digested in 100 mM EPPS, pH 8.5 containing 1 μg of trypsin (Promega) (overnight at 37 °C). Digests buffer was removed and 5 μL of TMTpro reagents (Thermo Fisher) was added to each solution for 1 hr at room temperature (25 °C). After incubating, the reaction was quenched by adding 1 μL of 5% (w/v) hydroxylamine. Labelled peptides were combined and subsequently desalted by C18 StageTips (Empore 3M).

Data were collected using an Orbitrap Fusion Lumos mass spectrometer (Thermo Fisher Scientific, San Jose, CA) coupled with a Proxeon EASY-nLC 1200 LC pump (Thermo Fisher Scientific). Peptides were separated on a 100 μm inner diameter microcapillary column packed with 35 cm of Accucore C18 resin (2.6 μm, 100 Å, Thermo Fisher Scientific). Peptides were separated using a 3 hr gradient of 6–22% acetonitrile in 0.125% formic acid with a flow rate of ~400 nL/min. Each analysis used an MS3-based TMT method. The data were acquired using a mass range of m/z 400 – 1400, resolution at 120,000, AGC target of 1×10^6, a maximum injection time 100 ms, dynamic exclusion of 180 seconds for the peptide measurements in the Orbitrap.

Data dependent MS2 spectra were acquired in the ion trap with a normalized collision energy (NCE) set at 35%, AGC target set to 2.0×10^5 and a maximum injection time of 120 ms. MS3 scans were acquired in the Orbitrap with a HCD collision energy set to 45%, AGC target set to 1.5×10^5, maximum injection time of 200 ms, resolution at 50,000 and with a maximum synchronous precursor selection (SPS) precursors set to 10.

In-house developed software was used to convert acquired mass spectrometric data from the .RAW file to the mzXML format. Erroneous assignments of peptide ion charge state and monoisotopic *m*/*z* were also corrected by the internal software. SEQUEST algorithm was used to assign MS2 spectra by searching the data against a protein sequence database including Mouse Uniprot Database (downloaded June 2017) and known contaminants such as mouse albumin and human keratins. A forward (target) database component was followed by a decoy component including all listed protein sequences. Searches were performed using a 20 ppm precursor ion tolerance and requiring both peptide termini to be consistent with trypsin specificity. 16-plex TMT labels on lysine residues and peptide N termini (+304.2071 Da) were set as static modifications and oxidation of methionine residues (+15.99492 Da) as a variable modification. An MS2 spectra assignment false discovery rate (FDR) of less than 1% was implemented by applying the target-decoy database search strategy. Filtering was performed using a linear discrimination analysis method to create one combined filter parameter from the following peptide ion and MS2 spectra properties: XCorr and ΔCn, peptide ion mass accuracy, and peptide length. Linear discrimination scores were used to assign probabilities to each MS2 spectrum for being assigned correctly and these probabilities were further used to filter the data set with an MS2 spectra assignment FDR to obtain protein identification FDR of less than 1%.

For reporter ion quantification, a 0.003 *m*/*z* window centred on the theoretical *m*/*z* value of each reporter ion was monitored for ions, and the maximum intensity of the signal to the theoretical *m*/*z* value was recorded. Reporter ion intensities were normalized by multiplication with the ion accumulation time for each MS2 or MS3 spectrum and adjusted based on the overlap of isotopic envelopes of all reporter ions. Following extraction of the reporter ion signal, the isotopic impurities of the TMT reagent were corrected using the values specified by the manufacturer's specification. Total signal-to-noise values for all peptides were summed for each TMT channel and all values were adjusted to account for variance and a total minimum signal-to-noise value of 200 was implemented.

Plasmids—Integrin αVβ5 ectodomain constructs were generated for recombinant protein production in mammalian cells as previously described[33,69,70]. In brief, soluble, heterodimeric αVβ5 construct was prepared from wild-type human αV and β5 cDNAs by PCR and standard molecular cloning techniques. αV subunit cDNA encoding the signal sequence and the ectodomain residues 32–991 was fused to a C-terminal peptide encoding an acidic α-helical coiled-coil region flanked by an N-terminal HRV3C protease recognition site and a C-terminal twin Strep-II tag and inserted into EcoR1 and BamH1 sites of the pcDNA3.1 vector. Similarly, a cDNA encoding the signal sequence and the ectodomain residues 24–717 of β5 was fused to a C-terminal sequence encoding a basic α-helical coiled-coil region flanked by an N-terminal HRV3C protease recognition site and a C-terminal 8xHis tag and inserted into EcoR1 and BamH1 sites of the pcDNA3.1

vector. Cys residues were introduced into both of the above constructs right in front of the HRV3C sites for formation of a disulfide bond potentially. For cellular assays, αVβ5 full-length constructs were purchased from Sino Biologicals (αV:HG11269-CY; β5:HG10779-CM). Irisin-mam and irisin-bac constructs used for recombinant protein production were generated as previously described[12,14]. Human Hsp90α and human Hsp70 full-length cDNAs were amplified by PCR from the plasmid purchased from Sino Biologicals (HSP90AA1: HG11445-CF; HSPA1A: HG11660-NF), and cloned into a C7 vector containing an HRV3C protease site and a 10 × His tag at the C-terminus using FX cloning system (Addgene 1000000039). Site-direct mutagenesis was used to introduce the single point mutation into Hsp90α. Human fibronectin 10^{th} FNIII domain DNA was synthesized by IDT and cloned into C7 vector containing a HRV3C protease site and a 10 × His tag at the C-terminus using FX cloning system (Addgene 1000000039).

Recombinant protein expression and purification—For protein expression in mammalian cells, 2.8×10^6 Expi293F cells (Life Technologies A14527) grown in 1 L Expi293F expression medium (Life Technologies A1435101) were transfected with 1mg DNA mixture containing 0.6 mg αV plasmid and 0.4 mg β5 plasmid, and 3mg sterile 25 kDa linear PEI mix in Opti-Plex Complexation Buffer (Life Technologies A4096801). Proteins were expressed at 37°C, 8% CO_2, >80% humidity with shaking at 125 rpm for 4 days. Enhancers (Life Technologies A14524) were added 22 hrs post transfection to boost protein expression.

For protein expression in E. coli, T7-express (NEB C2566) *E. coli* was transformed with the corresponding plasmid (Hsp90α, irisin-bac and FN10) and was grown in Terrific Broth until OD_{600} reached 2.5. 0.2 mM IPTG was added to induce protein expression at 22°C for 10 hrs.

For αVβ5 ectodomain protein (WT and mutants) purification from Expi293F cells, all of the following steps were performed at 4°C or on ice. Cells were pelleted at 600 × g for 20 min, and the medium was subjected to an additional 2 hrs of centrifugation at 1000 × g. The supernatant was filtered through 0.22 μm filter unit and was concentrated 10-fold using Tangential Filtration System with 50,000 kDa MWCO (Paul) before being applied to Ni-Excel affinity column (Cytiva 17371201) equilibrated in PB (10 mM Hepes pH7.4, 150 mM NaCl, 5 mM $CaCl_2$). After thorough washes with PB, the column was eluted with PB supplemented with 500 mM imidazole. The eluted protein was subsequently applied to Strep-Tactin column (IBA 2–1208) equilibrated in PB. After thorough washes with PB, the column was either: 1) treated with HRV3C protease in PB (at 1:100 enzyme to substrate molar ratio) for 16 hrs at 4°C followed by 3 column PB washes to obtain unclasped and untagged αVβ5; or 2) eluted with strep elution buffer (PB + 5 mM dethiobiotin) to obtain clasped and tagged αVβ5. For the highly purified material, protein was then loaded onto MonoQ ion exchange column (Cytiva 17516701) and eluted with a salt gradient (50 mM to 500 mM NaCl with 10 mM Tris at pH7.4). The peak fractions containing αVβ5 ectodomain were concentrated with 50,000 MWCO Amicon Ultra-15 filter unit (Millipore) before further purification through Superdex 200 10/300 GL gel-filtration column (Cytiva 17517501) equilibrated with Mg/Ca buffer (10 mM Hepes pH7.4, 150 mM NaCl, 1 mM

$MgCl_2$, 1 mM $CaCl_2$). Protein was further concentrated to >5 μM before being aliquoted, frozen in liquid nitrogen, and stored at −80°C. In all cases, the Hepes pH given is at 23°C.

For purification of Hsp90α and its mutant, FN10 and irisin-bac, all following steps were performed at 4°C or on ice. Cells were pelleted by centrifugation at 600 × g for 20 min at 4°C. Supernatant was removed and the cell pellet was washed once with PBS and resuspended in EB (100 mM Tris pH 8, 500 mM NaCl, 20 mM imidazole, 0.5 mM TCEP, 10% glycerol, 1 × Halt Protease Inhibitors (Thermo Fisher Scientific 78439)). Resuspended cells were then sonicated for 45 min (5 s on and 10 s off pulse) at 50% amplitude. Cell debris was removed by ultracentrifugation at 185,000 × g for 1 h. For Hsp90α and FN10, the supernatant was passed through Ni-NTA (ThermoFisher Scientific 25214) column, followed by thorough washes with WB (10 mM Tris pH 8, 250 mM NaCl, 40 mM imidazole, 0.5 mM TCEP). For Hsp90α, the column was then thoroughly washed with Mg^{2+}/ATP buffer (100 mM Tris pH7.4, 50 mM KCl, 5 mM ATP, 25 mM $MgCl_2$, 500 mM sucrose and 25% glycerol), followed by a minimum wash step with WB. The column was then treated with HRV3C protease in WB (at 1:100 enzyme to substrate molar ratio) for 16 hrs at 4°C, followed by 3 column volume WB washes to obtain the untagged Hsp90α and FN10. For irisin-bac, the supernatant was passed through Pierce Glutathione Argarose (Thermo Scientific 16100) column, followed by thorough washes with WBG (10 mM Tris pH 8, 250 mM NaCl, 0.5 mM TCEP). The column was then treated with HRV3C protease in WBG (at 1:100 enzyme to substrate molar ratio) for 16 hrs at 4°C followed by 3 column volume WBG wash to obtain untagged irisin-bac. The eluted proteins were concentrated with 30,000 MWCO (for Hsp90α) or 3,000 MWCO (for FN10 and irisin-bac) Amicon Ultra-15 filter unit (Millipore) before further purification through Superdex 200 10/300 GL gel-filtration column (Cytiva 17517501) equilibrated with FPLC buffer (10 mM Hepes pH7.4, 150 mM NaCl, 10% glycerol). Proteins were further concentrated to > 50 μM before being aliquoted, frozen in liquid nitrogen, and stored at −80°C. In all cases, Hepes pH given is at 23°C. A portion of the prepared Hsp90α planned for mammalian cell culture treatment was further purified using Toxin eraser Endotoxin Removal Kit (Gene Script L00338), and the level of endotoxin was measured using Toxin Sensor Chromogenic LAL Endotoxin Assay Kit (GeneScript L00350). The endotoxin-free Hsp90α was dialyzed into PBS and aliquoted, frozen in liquid nitrogen, and stored at −80°C

For biochemical reconstitution of the αVβ5/Hsp90α complex in stoichiometry, 1 μM clasped and tagged αVβ5 was incubated with 20 μM untagged Hsp90α in Mg/Ca buffer with end-over-end mixing at 4°C for 5 hrs. Protein mix was purified through TALON Metal Affinity column (Takara 635503) equilibrated in Mg/Ca buffer with extensive Mg/Ca buffer washing. The eluted protein complex was concentrated with 100,000 MWCO Amicon Ultra-15 filter unit (Millipore) before further purification through Superdex 200 10/300 GL gel-filtration column (Cytiva 17517501) equilibrated with Mg/Ca buffer. Protein complex was further concentrated to >5 μM before being aliquoted, frozen in liquid nitrogen, and stored at −80°C.

Proteins were dialyzed into the corresponding assaying buffers overnight at 4°C before the individual experiments were conducted.

Protein binding assays—Biolayer Inferometry (BLI) measurements were conducted by Octet RED384. 5 nM clasped and tagged αVβ5 was immobilized on Streptavidin biosensors (FortéBio 18–5019) and binding kinetics was measured with varying amounts of irisin in the Mg/Ca buffer. Data analysis HT software was used for the fitting and K_d calculations.

For TALON pull-down of purified Hsp90α (WT or mutant) or Hsp70, 1 μM clasped and tagged αVβ5 or control peptide dimer (HRV3C-acidic stretch-2xstrepII/HRV3C-basic stretch-8xHis) was incubated with 2 μM untagged Hsp90α (WT or mutant) or Hsp70 in Mg/Ca buffer with end-over-end mixing at 4°C for 1hr. Separately, 0.2 volumes of 50% TALON Metal Affinity bead slurry (Takara 635503) was washed in the Mg/Ca buffer before adding to protein mix. After 1 hr incubation at 4°C, beads were washed with the Mg/Ca buffer. The bead pellet was probed by either Coomassie staining or by western blot with anti-Hsp90α antibody (Invitrogen PA3–013) or anti-Hsp70 antibody (Invitrogen MA3–006). For TALON pull-down of purified Hsp90α recharged with different nucleotides, 10 μM Hsp90α was incubated with 1mM EDTA on ice for 5 min and dialyzed into DB (10 mM Hepes pH7.4, 150 mM NaCl, 5 mM $MgCl_2$) to obtain Hsp90α-apo. 1 mM ATP, AMP-PNP or ADP was then added into the αVβ5/Hsp90α mix for the pull-down assay.

For immuno-precipitation from cell extracts, SK-Mel2 cells were chilled on ice and incubated with 5 μg/mL anti-Hsp90α (Invitrogen PA3–013) for 1 hr at 4°C with shaking (7 see-saw movements per minute). The cells were than washed with cold PBS and lysed with prechilled IP buffer (50 mM Hepes pH7.4, 150 mM NaCl, 1% Triton X-100, 0.1% Na-deoxycholate, protease inhibitor cocktail (Roche 11873580001), PhosStop (Roche 49068450001), Pierce Universal Nuclease (Thermo Fisher Scientific 88700)). Cell debris was removed by centrifugation at 17,000 × g for 20 min at 4°C. The supernatant was then incubated with Protein A beads (Thermo Scientific 20333) equilibrated in IP buffer for 3 hrs. Beads were washed with the IP buffer, and the bound proteins were eluted with the SDS sample buffer. They were then resolved by SDS-PAGE, and probed with anti-Hsp90α (Invitrogen PA3–013), anti-αV (Cell Signaling 60896) or anti-β5 (Abcam ab184312).

For immuno-precipitation from iWAT, fat pads were harvested at the indicated time points and homogenized in chilled IP buffer as mentioned above using Polytron at 1,200 rpm for 2 min. The lysates were placed on ice for 30 min followed by centrifugation at 17,000 × g for 30 min at 4°C. The supernatant under the top fat layer was taken using a needle syringe, and cleaned up by 3 hrs of incubation with Protein A beads (Thermo Scientific 20333) equilibrated in IP buffer. The protein concentration of the supernatant was measured by Pierce Detergent Compatible Bradford Assay Reagent (Thermo Scientific 1863028), and 200 μg of total protein from each sample was used for incubation with anti-αV (Cell Signaling 60896) antibody or anti-His (Abcam ab9108) antibody (control) overnight at 4°C with end-over-end rotation, followed by 3 hrs of incubation with Protein A beads. The beads were then washed with the IP buffer, and the bound proteins were eluted with the SDS sample buffer. They were then resolved by SDS-PAGE, and probed with anti-Hsp90α (Invitrogen PA3–013) and anti-αV (R&D Systems AF1219).

Fluorescence polarization anisotropy measurements were conducted using irisin or FN10 labeled with Alexa Fluor 488 (A488), as previously described[71]. For the anisotropy binding

assays, 50 nM A488 labeled ligand proteins were mixed with varying concentrations of unlabeled receptor proteins or protein complexes dialyzed into the indicated buffers. For the anisotropy competition binding assay, 50 nM A488 labeled ligand proteins and fixed concentrations of the indicated receptor proteins or protein complexes dialyzed into the indicated buffers were mixed with varying concentrations of unlabeled ligand competitor proteins dialyzed into the indicated assaying buffers. Fluorescence anisotropy was measured using the Clariostar plate reader. Binding curves were fit using standard hyperbolic saturation fitting[72]. The K_d^{app} values were calculated based on[73–75].

MicroScale Thermophoresis (MST) was conducted using recombinant αVβ5 and A488-irisin in the presence of Mn^{2+} (10 mM Hepes pH 7.4, 150 mM NaCl, 1 mM $MnCl_2$). Total molar concentration of proteins were kept the same (1 μM) and varying αVβ5 to A488-irisin ratios (1:10, 1:7, 1:3, 1:1, 3:1, 7:1, and 10:1) were tested using standard treated capillaries (NanoTemper K002) and responses were measured using Monolith NT.115pico.

Detection of integrin signaling in HEK293T cells—For testing integrin signaling in HEK293T, cells were seeded onto the 10 cm dishes (4×10^6 cells/dish) and incubated at 37°C, 5% CO_2 overnight. Cells were then transfected with either 10 μg of control plasmid, or 10 μg of DNA mixture containing 0.6 μg of full-length αV, 0.4 μg of full-length β5 and 9 μg of control plasmid, as well as 24 μL Lipofectamine 2000 (Invitrogen 11668500), followed by 6 hrs of incubation. The transfected cells were then split into 6-well dishes (400,000 cells/well) and incubated overnight. Prior to irisin and/or Hsp90α treatment, cells were switched into FreeStyle293 expression medium (Life Technologies 12338–018) followed by 4–5 hrs of incubation. For cells that received Hsp90α, 1 nM Hsp90α was added directly into the cultures 1 hr before the irisin treatment, and then irisin was applied to the cells to the indicated final doses with minimum mechanical disturbance. Medium was removed after 5 minutes and cells were lysed with Pierce RIPA buffer (Thermo Scientific 89900), supplemented with Protease inhibitor cocktail (Roche 11836170001), PhosStop (Roche 04906837001) and Pierce Universal Nuclease (Thermo Fisher Scientific 88700). Cell lysates were scraped off the dishes and centrifuged at 17,000 × g for 10 min at 4°C. The protein concentration of the supernatant was measured by Pierce Detergent Compatible Bradford Assay Reagent (Thermo Scientific 1863028), and 10 μg of total protein from each sample was loaded and resolved by SDS-PAGE. Total FAK and the FAK phosphorylated at Y397 site (pFAK Y397) were probed with anti-FAK (Cell Signaling 3285) and anti-pFAK (Cell Signaling 3283).

For testing integrin signaling in iWAT, wild type 8-week C57BL/6J mice cells were given anti-Hsp90α (Enzo ADI-SPA-830, 500 μg/kg) antibody or control IgG (R&D Systems MAB002) injection subcutaneously. After 24 hrs, the mice were given a bolus injection of recombinant irisin (5 mg/kg) directly into the inguinal fat pads. iWAT was harvested 20 min after irisin injection and was homogenized using Polytron at 1200 rpm for 2 min in Pierce RIPA buffer (Thermo Scientific 89900), supplemented with Protease inhibitor cocktail (Roche 11836170001), PhosStop (Roche 04906837001) and Pierce Universal Nuclease (Thermo Fisher Scientific 88700). Tissue lysates were then centrifuged at 17,000 × g for 30 min at 4°C and the supernatant was taken using a needle syringe to avoid disturbing the top fat layer. The protein concentration of the supernatant was measured by Pierce

Detergent Compatible Bradford Assay Reagent (Thermo Scientific 1863028), and 10 μg of total protein from each sample was loaded and resolved by SDS-PAGE. Antibodies used for integrin signaling probing: anti-FAK (Cell Signaling 3285), anti-pFAK (Cell Signaling 3283), anti-CREB (Cell Signaling 9104), anti-pCREB (Cell Signaling 9198), anti-Src (Cell Signaling 2108), and anti-pSrc (Cell Signaling 6943).

Gene expression analysis by qRT-PCR—Total RNA was isolated from inguinal fat tissues after 45 min of irisin injection using TRIzol reagent (Invitrogen, 15596018) and RNeasy Mini purification kit (Qiagen, 74104) according the manufactures protocol. Tissues were homogenized in TRIzol reagent using a bead homogenizer for 20 min at max speed (Qiagen, TissueLyser II). DNA was digested on column using RNase-Free DNase Set (Qiagen, 79254). RNA was reversely transcribed using High-Capacity cDNA Reverse Transcription kit with RNase Inhibitor (Applied Biosystems, 4374966) and gene expression was determined by quantitative PCR (QuantStudio™ 6 Pro Real-Time PCR System, 384-well). Briefly, cDNA was mixed with 250–500 nmol primers and GoTaq qPCR System (Promega, A6002). Relative mRNA levels of the gene of interests were normalized to mRNA level of *Rplp0*. If not stated otherwise, primer sequences were chosen from PrimerBank[76–79]. Used primers and sequences: UCP1: CACCTTCCCGCTGGACACT and CCCTAGGACACCTTTATACCTAATGG; Dio2: AATTATGCCTCGGAGAAGACCG and GGCAGTTGCCTAGTGAAAGGT; Cidea: TGACATTCATGGGATTGCAGAC and GGCCAGTTGTGATGACTAAGAC; PGC1α: CCCTGCCATTGTTAAGACC and TGCTGCTGTTCCTGTTTTC; ALPL: TCAACACCAATGTAGCCAAGA and GTAGCTGGCCCTTAAGGATTC; Cox8b: GAACCATGAAGCCAACGACT and GCGAAGTTCACAGTGGTTCC; Rplp0: GGAGTGACATCGTCTTTAAACCCC and TCTGCTCCCACAATGAAGCA.

Fixed cell imaging and quantification—For irisin binding in HEK293T cells, cells were transfected as described above. The transfected cells were then split into the MatTek dishes (MatTek Life Sciences P35G-1.5–14-C) (200,000 cells/dish) and incubated overnight in the medium without phenol red. The next day, the cells were switched into FreeStyle293 expression medium (Life Technologies 12338–018) for 4–5 hrs. For the 1 hr Hsp90α pretreatment, 2 nM recombinant Hsp90α was added directly into the medium. The cells were then switched into prewarmed FreeStyle293 expression medium containing 2 nM A488-irisin for 5 min. After exactly 5min, medium was removed and cells were immediately fixed with 4% paraformaldehyde (Electron Microscopy Sciences 15710) at room temperature for 20 min. Cells were then washed with PBS and stained with DAPI (Calbiochem 268298) without permeabilization for 30 min at room temperature in the dark, followed by PBS wash. For irisin binding in SK-Mel2 cells, cells were chilled on ice and then were given control antibody (R&D MAB002) or anti-Hsp90α (Enzo ADI-SPA-830-F) (1:50 dilution) in cold medium for 1 hr at 4°C. Cells were washed with PBS and then switched into A647-irisin-containing warm FreeStyle293 medium for irisin binding following the same procedure described above. For immunostaining of cell surface Hsp90α, SK-Mel2 cells were seeded onto the MatTek dishes (400,000 cells/dish). After overnight incubation, cells were chilled on ice and then were given control antibody (R&D MAB002) or Hsp90α antibody (Enzo ADI-SPA-830-F) (1:50 dilution) in cold PBS for 1 hr on ice.

Cells were washed with cold PBS and fixed with 4% paraformaldehyde at room temperature for 20 min. After PBS wash, cells were incubated with A647-anti-mouse IgG (Invitrogen A21235) for 1 hr at room temperature followed by DAPI (Calbiochem 268298) staining in dark for 30 min. Cells were finally washed into PBS. Cells were imaged in PBS using Yokogawa spinning disc confocal on an inverted Nikon Ti fluorescence microscope and Hamamatsu ORCA-R_2 cooled CCD camera. Images were taken on the middle z-plane of the cells.

The number of A647-positive cells was quantified in confocal 640 nm channel based on the mean intensity values of the whole cell area (I_c, referring to the bright field) and the nucleus region (I_n, referring to the DAPI staining). Control dish with only DAPI staining was used to set up the baseline (I_b). $I_b = (I_c - I_n) /N$; N is the total number of the cells quantified. Cells with their ($I_c - I_n$) value above I_b were counted as positive. For the Hsp90α IF experiment, one Region of Interest (ROI) from each one biological replicate (total four biological repeats) was taken for quantification. For the A647-irisin binding experiment, three ROIs from three biological replicates were taken for quantification.

Cell viability assay—Crystal violet assay was used for quantification of cell viability. SK-Mel2 cells were seeded onto 24-well dishes (50,000 cells/well) and incubated overnight. Indicated amounts of irisin were added directly into the culture and cells were incubated for 24 hrs. Cells were then washed with PBS and stained with crystal violet solution for 15 min at room temperature followed by thorough washes with milliQ water. The stained cells were incubated in methanol supplemented with 10% acetic acid for 20 min, and the optical density at OD_{570} was measured using the Clariostar plate reader, and final OD_{570} values of the wells with cells were obtained by subtracting the average OD_{570} of the wells without cells.

Negative-stain electron microscopy—Hsp90α was diluted to a concentration of 0.02 mg/mL. To improve structural intactness of Hsp90α on the grids, we added 0.1% glutaraldehyde to the sample and incubated for 30 min on ice. Crosslinked and non-crosslinked Hsp90α samples were then applied onto glow-discharged continuous carbon grids (Electron Microscopy Sciences, Inc.), respectively. After 1 min of adsorption, the grids were blotted with filter paper to remove excess sample, and immediately washed twice with 4 μL of 1.5% uranyl formate solution followed by an incubation with 4 μL of 1.5% uranyl formate solution for additional 90 s. The grids were then further blotted with filter paper to remove the uranyl formate solution, air dried at room temperature, and examined with a Tecnai T12 electron microscope (Thermo Fisher Scientific) equipped with an LaB6 filament and operated at 120-kV acceleration voltage, using a nominal magnification of 69,000 × at a pixel size of 1.68 Å.

Cryo-EM and Image Processing—Cryo-EM grids of αVβ5 or αVβ5/Hsp90α were prepared using a Vitrobot Mark IV (Thermo Fisher Scientific). 3 μL aliquots of purified complex at concentrations between 0.5 and 0.8 mg/mL were applied onto glow-discharged C-flat holey carbon grids (R1.2/1.3, 400 mesh copper, Electron Microscopy Sciences). The grids were blotted for 6 s with a blot force of 15 and 100% humidity before being plunged into liquid ethane cooled by liquid nitrogen.

Images were acquired on a Titan Krios microscope equipped with a BioQuantum K3 Imaging Filter (slit width 25 eV) and a K3 direct electron detector (Gatan) and operating at an acceleration voltage of 200 kV. Images were recorded at a defocus range of −1.8 μm to −2.5 μm with a nominal magnification of 36,000 ×, resulting in a pixel size of 1.1 Å. Each image was dose-fractionated into 50 movie frames with a total exposure time of 4.5 s, resulting in a total dose of ~58.4 electrons per $Å^2$. SerialEM was used for data collection[80].

Images were processed using cryoSPARC[81]. For method 1, using template-free blob picker in cryoSPARC, 294,676 particles of αVβ5 were picked from 1,100 motion-corrected micrographs and extracted from the micrographs to run 2D classification. 148,637 particles were retained following 2D classification after selecting classes with well-resolved features. 367,732 particles of αVβ5/Hsp90α were picked from 1,171 motion-corrected micrographs and 193,293 particles were retained following 2D classification after selecting classes. Then, for both selected particles of αVβ5 and αVβ5/Hsp90α, we randomly split them at the same number of 140,000. For each dataset with 140,000 particles, we performed a 2D classification with 100 classes, respectively. Based on the 2D classes, we analyzed and calculated the “open”, “likely open”, “extended closed” and “closed” states of particles. For method 2, 6 2D classes generated from αVβ5 using blob picking, which contained “open”, “extended closed” and “closed” states, were used as templates to pick particles from both αVβ5 and αVβ5/Hsp90α micrographs. After selecting classes from 2D classification, total number of 314,469 αVβ5 particles and 313,849 αVβ5/Hsp90α particles were analyzed into “open”, “likely open”, “extended closed” and “closed” states, respectively. Method 3 followed a similar scheme to that described above for method 2, but the templates were generated from αVβ5/Hsp90α using blob picking. 330,301 particles of αVβ5 and 324,872 particles of αVβ5/Hsp90α were analyzed into “open”, “likely open”, “extended closed” and “closed” states, respectively.

Size-exclusion chromatography and multiangle light scattering (SEC-MALS)—Absolute molecular weights of irisin-mam and its conjugated glycan were determined using MALS coupled in-line with size-exclusion chromatography. 100 μg albumin (Thermo Scientific 23209) or irisin-mam was loaded onto Superdex 200 column equilibrated in 10 mM Hepes pH7.4, 150 mM NaCl. Light scattering from the column eluent was recorded at 16 different angles using a DAWN-HELEOS MALS detector (Wyatt Technology Corp.) operating at 658 nm. The detectors at different angles were calibrated using albumin (Thermo Scientific 23209). Protein concentration of the eluent was determined using an in-line Optilab DSP Interferometic Refractometer (Wyatt Technology Corp.). The weight-averaged molecular weight of species within defined chromatographic peaks was calculated using the ASTRA7 software (Wyatt Technology Corp.), by construction of Debye plots ($KC/R\theta$ versus $\sin^2[\theta/2]$) at 1^{-s} data intervals. The weight-averaged molecular weight was then calculated at each point of the chromatographic trace from the Debye plot intercept and an overall average molecular weight was calculated by averaging across the peak. Two concentration detectors (RI and UV) were used simultaneously during the MALS data collection and Protein Conjugate Analysis[82,83] was applied to SEC-MALS data using glycan dn/dc value of 0.145 mg/L.

Hydrogen/Deuterium exchange (HDX) mass spectrometry—In addition to the following descriptions, comprehensive experimental details and parameters are provided in Data S1 in the recommended[68] tabular format. All HDX-MS data have been deposited to the ProteomeX change Consortium via the PRIDE[68] partner repository with the dataset identifier PXD035397.

Deuterium labeling: for integrin protection, 20 μM irisin-His (from mammalian cells) was mixed with 4 μM αVβ5 ectodomain protein in Mn-buffer (10 mM Hepes pH7.4, 150 mM NaCl, 1 mM $MnCl_2$, H_2O); for irisin protection, 20 μM αVβ5 ectodomain protein was mixed with 4 μM irisin-His (from mammalian cells) in Mn-buffer. 20 μM irisin alone or αVβ5 alone were used as the "Apo" conditions. Deuterium labeling was initiated with an 18-fold dilution into D_2O buffer (18 μL, 10 mM Hepes pD 7.43, 150 mM NaCl, 1 mM $MnCl_2$, 99.9% D_2O) at 23 °C. After each labeling time (10 seconds, 10 minutes, and 4 hours) at 23 °C, the labeling reaction was quenched with the addition of 19 μL of ice-cold quenching buffer (200 mM potassium phosphate, pH 2.44, 4 M guanidinium chloride, 0.72 M TCEP, H_2O) and held on ice for 1 minute prior to LC/MS analysis.

LC/MS: Deuterated and control samples were digested online at 15 °C using an in-house-packed pepsin column. The cooling chamber of the UPLC system, which housed all the chromatographic elements, was held at 0.0 ± 0.1 °C for the entire time of the measurements. Peptides were trapped and desalted on a VanGuard Pre-Column trap [2.1 mm × 5 mm, ACQUITY UPLC BEH C18, 1.7 μm (Waters, 186002346)] for 3 minutes at 100 μL/min, eluted from the trap using a 5%–35% gradient of acetonitrile over 10 minutes at a flow rate of 100 μL/min, and separated using an ACQUITY UPLC HSS T3, 1.8 μm, 1.0 mm × 50 mm column (Waters, 186003535). Mass spectra were acquired using a Waters Synapt G2-Si $HDMS^E$ mass spectrometer in ion mobility mode. A conventional electrospray source was used, and the instrument was scanned over the range 50 to 2000 m/z. The error of determining the deuterium levels was ± 0.25 Da in this experimental setup. Deuterium levels were not corrected for back exchange and thus reported as relative [84].

HDX-MS data processing.: Peptides were identified from replicate $HDMS^E$ analyses (as detailed in the Data S1) of undeuterated control samples using PLGS 3.0.1 (Waters Corporation). The peptides identified in PLGS were filtered and processed with DynamX 3.0 software (Waters Corporation). All spectra were inspected manually. The relative amount of deuterium in each peptide was determined with the software by subtracting the centroid mass of the undeuterated form of each peptide from the deuterated form, at each time point, for each condition. These deuterium uptake values were used to generate all uptake graphs and difference maps.

Modeling and molecular dynamics simulations—The best ranked AlphaFold model of the integrin αVβ5 heterodimer and the crystal structure of the irisin protein (PDB 4LSD) were subjected to individual molecular dynamics runs. Each protein was prepared using CHARMM-GUI's Solution Builder for the integrin αVβ5 model, as an initial step, Mn^{2+} ions were added to the model based on their approximate positions taken from the integrin αVβ3 crystal structure (PDB 1M1X). Adequate protonation was assigned using the ProteinPrepare web server, at a pH of 7.4. The protein was placed in a rectangular

TIP3P waterbox and neutralized, with an additional 150 mM NaCl added in order to properly replicate cellular conditions. The prepared system was minimized and equilibrated for 1ns (NVT ensemble) and further subjected to a 360 ns production run (NPT ensemble, 298.15K). From the resulting trajectory, 35 snapshots were extracted at equal intervals, using VMD. In the case of irisin (PDB 4LSD), we first removed all crystallographic water molecules and only kept chain A from the initial structure. The resulting structure was prepared using a similar protocol to integrin αVβ5, with a production run of 500 ns. The first 150 ns of the production run trajectory were discarded and then 35 snapshots were extracted at equal intervals from the remaining 350 ns. All MD simulations and further clustering were conducted using the AMBER 2018 with the FF14SB forcefield and AmberTools.

Chain B: Irisin amino acid sequence used for the modeling:

MSPSAPVNVTVRHLKANSAVVSWDVLEDEVVIGFAISQQKKDVRMLRFIQEVNTTT
RSCALWDLEEDTEYIVHVQAISIQGQSPASEPVLFKTPREAE

Chain A: Integrin αVβ5 amino acid sequence used for the modeling (β5 is in *italic*):

MAFPPRRRLRLGPRGLPLLLSGLLLPLCRAFNLDVDSPAEYSGPEGSYFGFAVDFFVP
SASSRMFLLVGAPKANTTQPGIVEGGQVLKCDWSSTRRCQPIEFDATGNRDYAKDDP
LEFKSHQWFGASVRSKQDKILACAPLYHWRTEMKQEREPVGTCFLQDGTKTVEYAP
CRSQDIDADGQGFCQGGFSIDFTKADRVLLGGPGSFYWQGQLISDQVAEIVSKYDPN
VYSIKYNNQLATRTAQAIFDDSYLGYSVAVGDFNGDGIDDFVSGVPRAARTLGMVYI
YDGKNMSSLYNFTGEQMAAYFGFSVAATDINGDDYADVFIGAPLFMDRGSDGKLQE
VGQVSVSLQRASGDFQTTKLNGFEVFARFGSAIAPLGDLDQDGFNDIAIAAPYGGED
KKGIVYIFNGRSTGLNAVPSQILEGQWAARSMPPSFGYSMKGATDIDKNGYPDLIVG
AFGVDRAILYRARPVITVNAGLEVYPSILNQDNKTCSLPGTALKVSCFNVRFCLKAD
GKGVLPRKLNFQVELLLDKLKQKGAIRRALFLYSRSPSHSKNMTISRGGLMQCEELI
AYLRDESEFRDKLTPITIFMEYRLDYRTAADTTGLQPILNQFTPANISRQAHILLDCGE
DNVCKPKLEVSVDSDQKKIYIGDDNPLTLIVKAQNQGEGAYEAELIVSIPLQADFIGV
VRNNEALARLSCAFKTENQTRQVVCDLGNPMKAGTQLLAGLRFSVHQQSEMDTSV
KFDLQIQSSNLFDKVSPVVSHKVDLAV*SPASSFHVLRSLPLSSKGSGSAGWDVIQMTP*
QEIAVNLRPGDKTTFQLQVRQVEDYPVDLYYLMDLSLSMKDDLDNIRSLGTKLAEE
MRKLTSNFRLGFGSFVDKDISPFSYTAPRYQTNPCIGYKLFPNCVPSFGFRHLLPLTDR
VDSFNEEVRKQRVSRNRDAPEGGFDAVLQAAVCKEKIGWRKDALHLLVFTTDDVPH
IALDGKLGGLVQPHDGQCHLNEANEYTASNQMDYPSLALLGEKLAENNINLIFAVTK
NHYMLYKNFTALIPGTTVEILDGDSKNIIQLIINAYNSIRSKVELSVWDQPEDLNLFFT
ATCQDGVSYPGQRKCEGLKIGDTASFEVSLEARSCPSRHTEHVFALRPVGFRDSLEV
GVTYNCTC

Docking—The resulting snapshots (35 for each protein) were further prepared using PDBTools in order to generate proper ensembles and submitted for docking to the HADDOCK web server. Docking was performed on the 2 resulting ensembles using the default parameters provided by the Guru interface: in the case of integrin αVβ5, active residues were defined based on the provided HDX-MS data. Passive residues were

selected automatically by HADDOCK, based on the proximity to active residues (see more information in Data S2). In the case of irisin, all residues in the structure were defined as active.

Final MD refinement stage—The best docking pose from the top ranked cluster (pose 1, cluster 2) was further subjected to a short MD simulation for an additional 100 ns to further optimize the αVβ5-irisin interaction. The resulting trajectory was clustered using AmberTools with the k-means clustering algorithm. The structures from the most populated clusters were visually inspected to select the final model of the αVβ5-irisin interaction.

Quantification and Statistical analysis—All data are represented as mean ± s.e.m. with at least 3 independent experiments. Fluorescence anisotropy binding curves were fit using KaleidaGraph 3.51. Statistical analysis was performed using GraphPad Prism 7. Differences between 2 means and among multiple means were assessed by unpaired two-tailed student *t* test and ANOVA, respectively. Assessments with $P < 0.05$ were considered significant. For proteomic data, Statistical analysis was performed using Perseus[85]. Total quantified proteins were filtered to remove unreviewed TrREMBL sequences and proteins quantified using a single peptide. Significant changes were determined using a permutation-based FDR with the following settings – FDR – 0.05, S0 – 0.1, and number of randomizations – 250.

Supplementary Material

Refer to Web version on PubMed Central for supplementary material.

Acknowledgements

We gratefully acknowledge the funding from the JPB Foundation (6293803). M. A is supported by the NIH F32 (1F32DK132864–01). H.Z is supported by BCMP-Merck Postdoctoral Fellowship. M.J.M. is funded by the Deutsche Forschungsgemeinschaft (DFG, German research foundation) – Projektnummer 461079553 and was funded by the NIH/NHLBI Training Program in Cardiovascular Research 5T32HL007374–41. We thank all the members of the Spiegelman lab for the helpful discussions. We acknowledge the Nikon Imaging Center at Harvard Medical School, the Center for Macromolecular Interactions at Harvard University, the Molecular Electron Microscopy Suite at Harvard Medical School, and the Cryo-EM Center at Harvard Medical School. We thank Dr. M. Amin Arnaout and Dr. Marc W. Kirschner for invaluable advice.

Reference

1. Myers J, Prakash M, Froelicher V, Do D, Partington S, and Atwood JE (2002). Exercise capacity and mortality among men referred for exercise testing. N Engl J Med 346, 793–801. 10.1056/NEJMoa011858. [PubMed: 11893790]
2. Fernandez-Marcos PJ, and Auwerx J (2011). Regulation of PGC-1alpha, a nodal regulator of mitochondrial biogenesis. Am J Clin Nutr 93, 884S–890. 10.3945/ajcn.110.001917. [PubMed: 21289221]
3. Puigserver P, Wu Z, Park CW, Graves R, Wright M, and Spiegelman BM (1998). A cold-inducible coactivator of nuclear receptors linked to adaptive thermogenesis. Cell 92, 829–839. 10.1016/s0092-8674(00)81410-5. [PubMed: 9529258]
4. Reutzel M, Grewal R, Dilberger B, Silaidos C, Joppe A, and Eckert GP (2020). Cerebral Mitochondrial Function and Cognitive Performance during Aging: A Longitudinal Study in NMRI Mice. Oxid Med Cell Longev 2020, 4060769. 10.1155/2020/4060769. [PubMed: 32377297]

5. Uldry M, Yang W, St-Pierre J, Lin J, Seale P, and Spiegelman BM (2006). Complementary action of the PGC-1 coactivators in mitochondrial biogenesis and brown fat differentiation. Cell Metab 3, 333–341. 10.1016/j.cmet.2006.04.002. [PubMed: 16679291]
6. Baar K, Wende AR, Jones TE, Marison M, Nolte LA, Chen M, Kelly DP, and Holloszy JO (2002). Adaptations of skeletal muscle to exercise: rapid increase in the transcriptional coactivator PGC-1. FASEB J 16, 1879–1886. 10.1096/fj.02-0367com. [PubMed: 12468452]
7. Correia JC, Ferreira DM, and Ruas JL (2015). Intercellular: local and systemic actions of skeletal muscle PGC-1s. Trends Endocrinol Metab 26, 305–314. 10.1016/j.tem.2015.03.010. [PubMed: 25934582]
8. Handschin C, Chin S, Li P, Liu F, Maratos-Flier E, Lebrasseur NK, Yan Z, and Spiegelman BM (2007). Skeletal muscle fiber-type switching, exercise intolerance, and myopathy in PGC-1alpha muscle-specific knock-out animals. J Biol Chem 282, 30014–30021. 10.1074/jbc.M704817200. [PubMed: 17702743]
9. Lin J, Wu H, Tarr PT, Zhang CY, Wu Z, Boss O, Michael LF, Puigserver P, Isotani E, Olson EN, et al. (2002). Transcriptional co-activator PGC-1 alpha drives the formation of slow-twitch muscle fibres. Nature 418, 797–801. 10.1038/nature00904. [PubMed: 12181572]
10. Norrbom J, Sundberg CJ, Ameln H, Kraus WE, Jansson E, and Gustafsson T (2004). PGC-1alpha mRNA expression is influenced by metabolic perturbation in exercising human skeletal muscle. J Appl Physiol (1985) 96, 189–194. 10.1152/japplphysiol.00765.2003. [PubMed: 12972445]
11. Bostrom P, Wu J, Jedrychowski MP, Korde A, Ye L, Lo JC, Rasbach KA, Bostrom EA, Choi JH, Long JZ, et al. (2012). A PGC1-alpha-dependent myokine that drives brown-fat-like development of white fat and thermogenesis. Nature 481, 463–468. 10.1038/nature10777. [PubMed: 22237023]
12. Schumacher MA, Chinnam N, Ohashi T, Shah RS, and Erickson HP (2013). The structure of irisin reveals a novel intersubunit beta-sheet fibronectin type III (FNIII) dimer: implications for receptor activation. J Biol Chem 288, 33738–33744. 10.1074/jbc.M113.516641. [PubMed: 24114836]
13. Jedrychowski MP, Wrann CD, Paulo JA, Gerber KK, Szpyt J, Robinson MM, Nair KS, Gygi SP, and Spiegelman BM (2015). Detection and Quantitation of Circulating Human Irisin by Tandem Mass Spectrometry. Cell Metab 22, 734–740. 10.1016/j.cmet.2015.08.001. [PubMed: 26278051]
14. Kim H, Wrann CD, Jedrychowski M, Vidoni S, Kitase Y, Nagano K, Zhou C, Chou J, Parkman VA, Novick SJ, et al. (2018). Irisin Mediates Effects on Bone and Fat via alphaV Integrin Receptors. Cell 175, 1756–1768 e1717. 10.1016/j.cell.2018.10.025. [PubMed: 30550785]
15. Lee P, Linderman JD, Smith S, Brychta RJ, Wang J, Idelson C, Perron RM, Werner CD, Phan GQ, Kammula US, et al. (2014). Irisin and FGF21 are cold-induced endocrine activators of brown fat function in humans. Cell Metab 19, 302–309. 10.1016/j.cmet.2013.12.017. [PubMed: 24506871]
16. Islam MR, Valaris S, Young MF, Haley EB, Luo R, Bond SF, Mazuera S, Kitchen RR, Caldarone BJ, Bettio LEB, et al. (2021). Exercise hormone irisin is a critical regulator of cognitive function. Nat Metab 3, 1058–1070. 10.1038/s42255-021-00438-z. [PubMed: 34417591]
17. Kam TI, Park H, Chou SC, Van Vranken JG, Mittenbuhler MJ, Kim H, A M., Choi YR., Biswas D., Wang J., et al. (2022). Amelioration of pathologic alpha-synuclein-induced Parkinson's disease by irisin. Proc Natl Acad Sci U S A 119, e2204835119. 10.1073/pnas.2204835119. [PubMed: 36044549]
18. Hynes RO (2002). Integrins: bidirectional, allosteric signaling machines. Cell 110, 673–687. 10.1016/s0092-8674(02)00971-6. [PubMed: 12297042]
19. Kadry YA, and Calderwood DA (2020). Chapter 22: Structural and signaling functions of integrins. Biochim Biophys Acta Biomembr 1862, 183206. 10.1016/j.bbamem.2020.183206. [PubMed: 31991120]
20. Campbell ID, and Humphries MJ (2011). Integrin structure, activation, and interactions. Cold Spring Harb Perspect Biol 3. 10.1101/cshperspect.a004994.
21. Springer TA, and Dustin ML (2012). Integrin inside-out signaling and the immunological synapse. Curr Opin Cell Biol 24, 107–115. 10.1016/j.ceb.2011.10.004. [PubMed: 22129583]
22. Li J, Su Y, Xia W, Qin Y, Humphries MJ, Vestweber D, Cabanas C, Lu C, and Springer TA (2017). Conformational equilibria and intrinsic affinities define integrin activation. EMBO J 36, 629–645. 10.15252/embj.201695803. [PubMed: 28122868]

23. Su Y, Xia W, Li J, Walz T, Humphries MJ, Vestweber D, Cabanas C, Lu C, and Springer TA (2016). Relating conformation to function in integrin alpha5beta1. Proc Natl Acad Sci U S A 113, E3872–3881. 10.1073/pnas.1605074113. [PubMed: 27317747]
24. Li J, and Springer TA (2018). Energy landscape differences among integrins establish the framework for understanding activation. J Cell Biol 217, 397–412. 10.1083/jcb.201701169. [PubMed: 29122968]
25. Li J, and Springer TA (2017). Integrin extension enables ultrasensitive regulation by cytoskeletal force. Proc Natl Acad Sci U S A 114, 4685–4690. 10.1073/pnas.1704171114. [PubMed: 28416675]
26. Ginsberg MH (2014). Integrin activation. BMB Rep 47, 655–659. 10.5483/bmbrep.2014.47.12.241. [PubMed: 25388208]
27. Ni H, Li A, Simonsen N, and Wilkins JA (1998). Integrin activation by dithiothreitol or Mn2+ induces a ligand-occupied conformation and exposure of a novel NH2-terminal regulatory site on the beta1 integrin chain. J Biol Chem 273, 7981–7987. 10.1074/jbc.273.14.7981. [PubMed: 9525896]
28. Xiong JP, Stehle T, Diefenbach B, Zhang R, Dunker R, Scott DL, Joachimiak A, Goodman SL, and Arnaout MA (2001). Crystal structure of the extracellular segment of integrin alpha Vbeta3. Science 294, 339–345. 10.1126/science.1064535. [PubMed: 11546839]
29. Xiao T, Takagi J, Coller BS, Wang JH, and Springer TA (2004). Structural basis for allostery in integrins and binding to fibrinogen-mimetic therapeutics. Nature 432, 59–67. 10.1038/nature02976. [PubMed: 15378069]
30. Anderson JM, Li J, and Springer TA (2022). Regulation of integrin alpha5beta1 conformational states and intrinsic affinities by metal ions and the ADMIDAS. Mol Biol Cell 33, ar56. 10.1091/mbc.E21-11-0536. [PubMed: 35108026]
31. Huhtala M, Heino J, Casciari D, de Luise A, and Johnson MS (2005). Integrin evolution: insights from ascidian and teleost fish genomes. Matrix Biol 24, 83–95. 10.1016/j.matbio.2005.01.003. [PubMed: 15890260]
32. Xiong JP, Stehle T, Zhang R, Joachimiak A, Frech M, Goodman SL, and Arnaout MA (2002). Crystal structure of the extracellular segment of integrin alpha Vbeta3 in complex with an Arg-Gly-Asp ligand. Science 296, 151–155. 10.1126/science.1069040. [PubMed: 11884718]
33. Nishida N, Xie C, Shimaoka M, Cheng Y, Walz T, and Springer TA (2006). Activation of leukocyte beta2 integrins by conversion from bent to extended conformations. Immunity 25, 583–594. 10.1016/j.immuni.2006.07.016. [PubMed: 17045822]
34. Wang X, Song X, Zhuo W, Fu Y, Shi H, Liang Y, Tong M, Chang G, and Luo Y (2009). The regulatory mechanism of Hsp90alpha secretion and its function in tumor malignancy. Proc Natl Acad Sci U S A 106, 21288–21293. 10.1073/pnas.0908151106. [PubMed: 19965370]
35. McCready J, Sims JD, Chan D, and Jay DG (2010). Secretion of extracellular hsp90alpha via exosomes increases cancer cell motility: a role for plasminogen activation. BMC Cancer 10, 294. 10.1186/1471-2407-10-294. [PubMed: 20553606]
36. Gopal U, Bohonowych JE, Lema-Tome C, Liu A, Garrett-Mayer E, Wang B, and Isaacs JS (2011). A novel extracellular Hsp90 mediated co-receptor function for LRP1 regulates EphA2 dependent glioblastoma cell invasion. PLoS One 6, e17649. 10.1371/journal.pone.0017649. [PubMed: 21408136]
37. Murshid A, Gong J, and Calderwood SK (2010). Heat shock protein 90 mediates efficient antigen cross presentation through the scavenger receptor expressed by endothelial cells-I. J Immunol 185, 2903–2917. 10.4049/jimmunol.0903635. [PubMed: 20686127]
38. Sidera K, Gaitanou M, Stellas D, Matsas R, and Patsavoudi E (2008). A critical role for HSP90 in cancer cell invasion involves interaction with the extracellular domain of HER-2. J Biol Chem 283, 2031–2041. 10.1074/jbc.M701803200. [PubMed: 18056992]
39. Backe SJ, Sager RA, Regan BR, Sit J, Major LA, Bratslavsky G, Woodford MR, Bourboulia D, and Mollapour M (2022). A specialized Hsp90 co-chaperone network regulates steroid hormone receptor response to ligand. Cell Rep 40, 111039. 10.1016/j.celrep.2022.111039. [PubMed: 35830801]

40. Cortes S, Baker-Williams AJ, Mollapour M, and Bourboulia D (2018). Detection and Analysis of Extracellular Hsp90 (eHsp90). Methods Mol Biol 1709, 321–329. 10.1007/978-1-4939-7477-1_23. [PubMed: 29177669]

41. Sager RA, Khan F, Toneatto L, Votra SD, Backe SJ, Woodford MR, Mollapour M, and Bourboulia D (2022). Targeting extracellular Hsp90: A unique frontier against cancer. Front Mol Biosci 9. 10.3389/fmolb.2022.982593.

42. Spinelli JB, Yoon H, Ringel AE, Jeanfavre S, Clish CB, and Haigis MC (2017). Metabolic recycling of ammonia via glutamate dehydrogenase supports breast cancer biomass. Science 358, 941–946. 10.1126/science.aam9305. [PubMed: 29025995]

43. Wiig H, Aukland K, and Tenstad O (2003). Isolation of interstitial fluid from rat mammary tumors by a centrifugation method. Am J Physiol Heart Circ Physiol 284, H416–424. 10.1152/ajpheart.00327.2002. [PubMed: 12388326]

44. Sullivan MR, Danai LV, Lewis CA, Chan SH, Gui DY, Kunchok T, Dennstedt EA, Vander Heiden MG, and Muir A (2019). Quantification of microenvironmental metabolites in murine cancers reveals determinants of tumor nutrient availability. Elife 8. 10.7554/eLife.44235.

45. Reddy A, Bozi LHM, Yaghi OK, Mills EL, Xiao H, Nicholson HE, Paschini M, Paulo JA, Garrity R, Laznik-Bogoslavski D, et al. (2020). pH-Gated Succinate Secretion Regulates Muscle Remodeling in Response to Exercise. Cell 183, 62–75 e17. 10.1016/j.cell.2020.08.039. [PubMed: 32946811]

46. Mittenbuhler MJ, Jedrychowski MP, Van Vranken JG, Sprenger HG, Wilensky S, Dumesic PA, Sun Y, Tartaglia A, Bogoslavski D, A, M., et al. (2023). Isolation of extracellular fluids reveals novel secreted bioactive proteins from muscle and fat tissues. Cell Metab 35, 535–549 e537. 10.1016/j.cmet.2022.12.014. [PubMed: 36681077]

47. Li W, Li Y, Guan S, Fan J, Cheng CF, Bright AM, Chinn C, Chen M, and Woodley DT (2007). Extracellular heat shock protein-90alpha: linking hypoxia to skin cell motility and wound healing. EMBO J 26, 1221–1233. 10.1038/sj.emboj.7601579. [PubMed: 17304217]

48. Sidera K, Samiotaki M, Yfanti E, Panayotou G, and Patsavoudi E (2004). Involvement of cell surface HSP90 in cell migration reveals a novel role in the developing nervous system. J Biol Chem 279, 45379–45388. 10.1074/jbc.M405486200. [PubMed: 15302889]

49. Becker B, Multhoff G, Farkas B, Wild PJ, Landthaler M, Stolz W, and Vogt T (2004). Induction of Hsp90 protein expression in malignant melanomas and melanoma metastases. Exp Dermatol 13, 27–32. 10.1111/j.0906-6705.2004.00114.x.

50. Stellas D, Karameris A, and Patsavoudi E (2007). Monoclonal antibody 4C5 immunostains human melanomas and inhibits melanoma cell invasion and metastasis. Clin Cancer Res 13, 1831–1838. 10.1158/1078-0432.CCR-06-1585. [PubMed: 17363539]

51. Danen EH, Jansen KF, Van Kraats AA, Cornelissen IM, Ruiter DJ, and Van Muijen GN (1995). Alpha v-integrins in human melanoma: gain of alpha v beta 3 and loss of alpha v beta 5 are related to tumor progression in situ but not to metastatic capacity of cell lines in nude mice. Int J Cancer 61, 491–496. 10.1002/ijc.2910610411. [PubMed: 7538977]

52. Sechler JL, Corbett SA, and Schwarzbauer JE (1997). Modulatory roles for integrin activation and the synergy site of fibronectin during matrix assembly. Mol Biol Cell 8, 2563–2573. 10.1091/mbc.8.12.2563. [PubMed: 9398676]

53. Southworth DR, and Agard DA (2008). Species-dependent ensembles of conserved conformational states define the Hsp90 chaperone ATPase cycle. Mol Cell 32, 631–640. 10.1016/j.molcel.2008.10.024. [PubMed: 19061638]

54. Frelinger AL 3rd, Du XP, Plow EF, and Ginsberg MH (1991). Monoclonal antibodies to ligand-occupied conformers of integrin alpha IIb beta 3 (glycoprotein IIb-IIIa) alter receptor affinity, specificity, and function. J Biol Chem 266, 17106–17111. [PubMed: 1894607]

55. Arroyo AG, Sanchez-Mateos P, Campanero MR, Martin-Padura I, Dejana E, and Sanchez-Madrid F (1992). Regulation of the VLA integrin-ligand interactions through the beta 1 subunit. J Cell Biol 117, 659–670. 10.1083/jcb.117.3.659. [PubMed: 1374069]

56. Kovach NL, Carlos TM, Yee E, and Harlan JM (1992). A monoclonal antibody to beta 1 integrin (CD29) stimulates VLA-dependent adherence of leukocytes to human umbilical vein

endothelial cells and matrix components. J Cell Biol 116, 499–509. 10.1083/jcb.116.2.499. [PubMed: 1370496]

57. Elices MJ, Urry LA, and Hemler ME (1991). Receptor functions for the integrin VLA-3: fibronectin, collagen, and laminin binding are differentially influenced by Arg-Gly-Asp peptide and by divalent cations. J Cell Biol 112, 169–181. 10.1083/jcb.112.1.169. [PubMed: 1986004]
58. Dransfield I, Cabanas C, Craig A, and Hogg N (1992). Divalent cation regulation of the function of the leukocyte integrin LFA-1. J Cell Biol 116, 219–226. 10.1083/jcb.116.1.219. [PubMed: 1346139]
59. Grenert JP, Sullivan WP, Fadden P, Haystead TA, Clark J, Mimnaugh E, Krutzsch H, Ochel HJ, Schulte TW, Sausville E, et al. (1997). The amino-terminal domain of heat shock protein 90 (hsp90) that binds geldanamycin is an ATP/ADP switch domain that regulates hsp90 conformation. J Biol Chem 272, 23843–23850. 10.1074/jbc.272.38.23843. [PubMed: 9295332]
60. Moran Jerabek-Willemsen TA, Randy Wanner, Heide Marie Roth, Stefan Duhr, Philipp Baaske, Dennis Breitsprecher(2014). MicroScale Thermophoresis: Interaction analysis and beyond. Journal of Molecular Strcuture 1077, 101–113.
61. Wang J, Su Y, Iacob RE, Engen JR, and Springer TA (2019). General structural features that regulate integrin affinity revealed by atypical alphaVbeta8. Nat Commun 10, 5481. 10.1038/s41467-019-13248-5. [PubMed: 31792290]
62. Hollingsworth SA, and Dror RO (2018). Molecular Dynamics Simulation for All. Neuron 99, 1129–1143. 10.1016/j.neuron.2018.08.011. [PubMed: 30236283]
63. Croset A, Delafosse L, Gaudry JP, Arod C, Glez L, Losberger C, Begue D, Krstanovic A, Robert F, Vilbois F, et al. (2012). Differences in the glycosylation of recombinant proteins expressed in HEK and CHO cells. J Biotechnol 161, 336–348. 10.1016/j.jbiotec.2012.06.038. [PubMed: 22814405]
64. Bohm E, Seyfried BK, Dockal M, Graninger M, Hasslacher M, Neurath M, Konetschny C, Matthiessen P, Mitterer A, and Scheiflinger F (2015). Differences in N-glycosylation of recombinant human coagulation factor VII derived from BHK, CHO, and HEK293 cells. BMC Biotechnol 15, 87. 10.1186/s12896-015-0205-1. [PubMed: 26382581]
65. Goh JB, and Ng SK (2018). Impact of host cell line choice on glycan profile. Crit Rev Biotechnol 38, 851–867. 10.1080/07388551.2017.1416577. [PubMed: 29262720]
66. Edwards DN, and Bix GJ (2019). Roles of blood-brain barrier integrins and extracellular matrix in stroke. Am J Physiol Cell Physiol 316, C252–C263. 10.1152/ajpcell.00151.2018. [PubMed: 30462535]
67. Ayloo S, and Gu C (2019). Transcytosis at the blood-brain barrier. Curr Opin Neurobiol 57, 32–38. 10.1016/j.conb.2018.12.014. [PubMed: 30708291]
68. Perez-Riverol Y, Bai J, Bandla C, Garcia-Seisdedos D, Hewapathirana S, Kamatchinathan S, Kundu DJ, Prakash A, Frericks-Zipper A, Eisenacher M, et al. (2022). The PRIDE database resources in 2022: a hub for mass spectrometry-based proteomics evidences. Nucleic Acids Res 50, D543–D552. 10.1093/nar/gkab1038. [PubMed: 34723319]
69. Takagi J, Erickson HP, and Springer TA (2001). C-terminal opening mimics 'inside-out' activation of integrin alpha5beta1. Nat Struct Biol 8, 412–416. 10.1038/87569. [PubMed: 11323715]
70. Xie C, Zhu J, Chen X, Mi L, Nishida N, and Springer TA (2010). Structure of an integrin with an alphaI domain, complement receptor type 4. EMBO J 29, 666–679. 10.1038/emboj.2009.367. [PubMed: 20033057]
71. Ramabhadran V, Hatch AL, and Higgs HN (2013). Actin monomers activate inverted formin 2 by competing with its autoinhibitory interaction. J Biol Chem 288, 26847–26855. 10.1074/jbc.M113.472415. [PubMed: 23921379]
72. Hulme EC, and Trevethick MA (2010). Ligand binding assays at equilibrium: validation and interpretation. Br J Pharmacol 161, 1219–1237. 10.1111/j.1476-5381.2009.00604.x. [PubMed: 20132208]
73. Benedetti MS, Boucher T, Carlsson A, and Fowler CJ (1983). Intestinal metabolism of tyramine by both forms of monoamine oxidase in the rat. Biochem Pharmacol 32, 47–52. 10.1016/0006-2952(83)90650-0. [PubMed: 6830619]
74. Marechal JD, Yu J, Brown S, Kapelioukh I, Rankin EM, Wolf CR, Roberts GC, Paine MJ, and Sutcliffe MJ (2006). In silico and in vitro screening for inhibition of cytochrome P450 CYP3A4 by

comedications commonly used by patients with cancer. Drug Metab Dispos 34, 534–538. 10.1124/dmd.105.007625. [PubMed: 16415122]

75. Burnett JC, Opsenica D, Sriraghavan K, Panchal RG, Ruthel G, Hermone AR, Nguyen TL, Kenny TA, Lane DJ, McGrath CF, et al. (2007). A refined pharmacophore identifies potent 4-amino-7-chloroquinoline-based inhibitors of the botulinum neurotoxin serotype A metalloprotease. J Med Chem 50, 2127–2136. 10.1021/jm061446e. [PubMed: 17417831]
76. Wang X, Spandidos A, Wang H, and Seed B (2012). PrimerBank: a PCR primer database for quantitative gene expression analysis, 2012 update. Nucleic Acids Res 40, D1144–1149. 10.1093/nar/gkr1013. [PubMed: 22086960]
77. Spandidos A, Wang X, Wang H, and Seed B (2010). PrimerBank: a resource of human and mouse PCR primer pairs for gene expression detection and quantification. Nucleic Acids Res 38, D792–799. 10.1093/nar/gkp1005. [PubMed: 19906719]
78. Spandidos A, Wang X, Wang H, Dragnev S, Thurber T, and Seed B (2008). A comprehensive collection of experimentally validated primers for Polymerase Chain Reaction quantitation of murine transcript abundance. BMC Genomics 9, 633. 10.1186/1471-2164-9-633. [PubMed: 19108745]
79. Wang X, and Seed B (2003). A PCR primer bank for quantitative gene expression analysis. Nucleic Acids Res 31, e154. 10.1093/nar/gng154. [PubMed: 14654707]
80. Schorb M, Haberbosch I, Hagen WJH, Schwab Y, and Mastronarde DN (2019). Software tools for automated transmission electron microscopy. Nat Methods 16, 471–477. 10.1038/s41592-019-0396-9. [PubMed: 31086343]
81. Punjani A, Rubinstein JL, Fleet DJ, and Brubaker MA (2017). cryoSPARC: algorithms for rapid unsupervised cryo-EM structure determination. Nat Methods 14, 290–296. 10.1038/nmeth.4169. [PubMed: 28165473]
82. Strop P, and Brunger AT (2005). Refractive index-based determination of detergent concentration and its application to the study of membrane proteins. Protein Sci 14, 2207–2211. 10.1110/ps.051543805. [PubMed: 16046633]
83. Pasternack SG, Veis A, and Breen M (1974). Solvent-dependent changes in proteoglycan subunit conformation in aqueous guanidine hydrochloride solutions. J Biol Chem 249, 2206–2211. [PubMed: 4274235]
84. Wales TE, and Engen JR (2006). Hydrogen exchange mass spectrometry for the analysis of protein dynamics. Mass Spectrom Rev 25, 158–170. 10.1002/mas.20064. [PubMed: 16208684]
85. Tyanova S, Temu T, Sinitcyn P, Carlson A, Hein MY, Geiger T, Mann M, and Cox J (2016). The Perseus computational platform for comprehensive analysis of (prote)omics data. Nat Methods 13, 731–740. 10.1038/nmeth.3901. [PubMed: 27348712]
86. Sun Y, Rahbani JF, Jedrychowski MP, Riley CL, Vidoni S, Bogoslavski D, Hu B, Dumesic PA, Zeng X, Wang AB, et al. (2021). Mitochondrial TNAP controls thermogenesis by hydrolysis of phosphocreatine. Nature 593, 580–585. 10.1038/s41586-021-03533-z. [PubMed: 33981039]

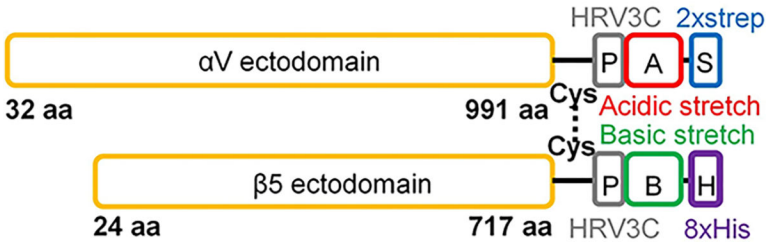

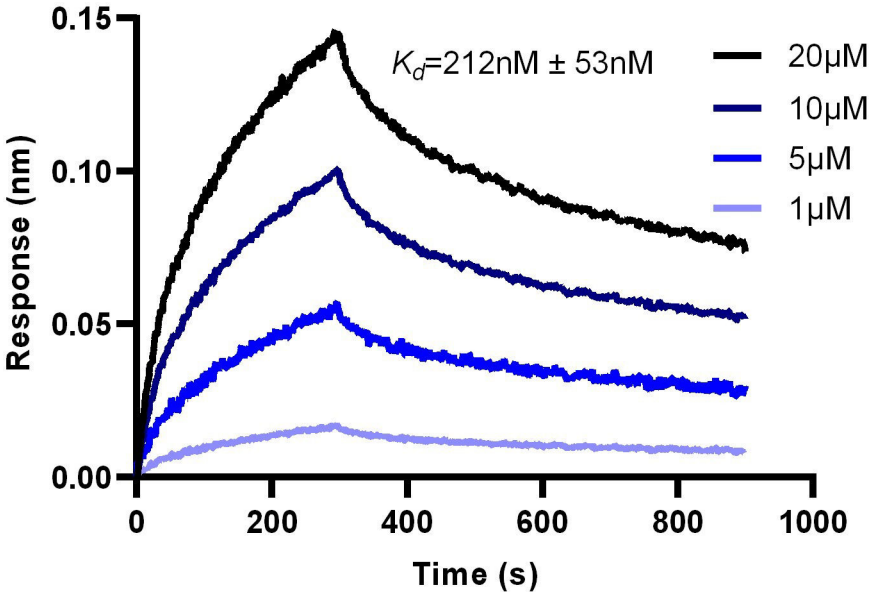

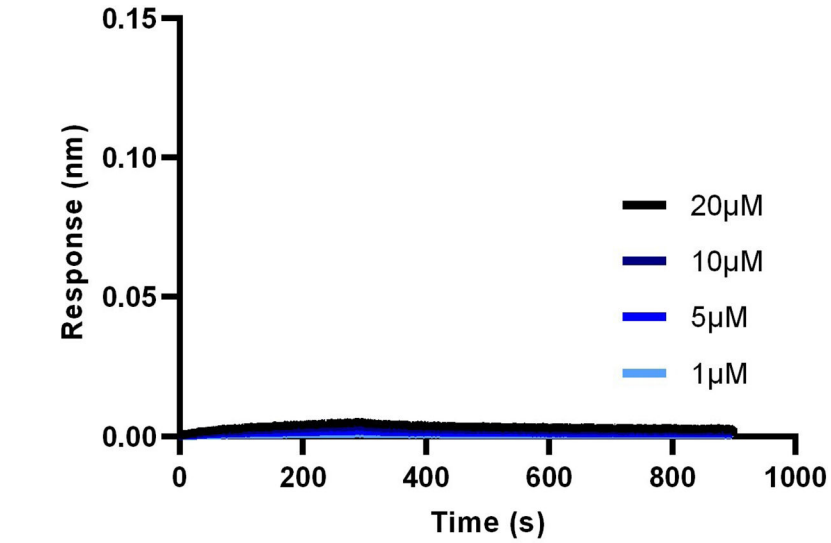

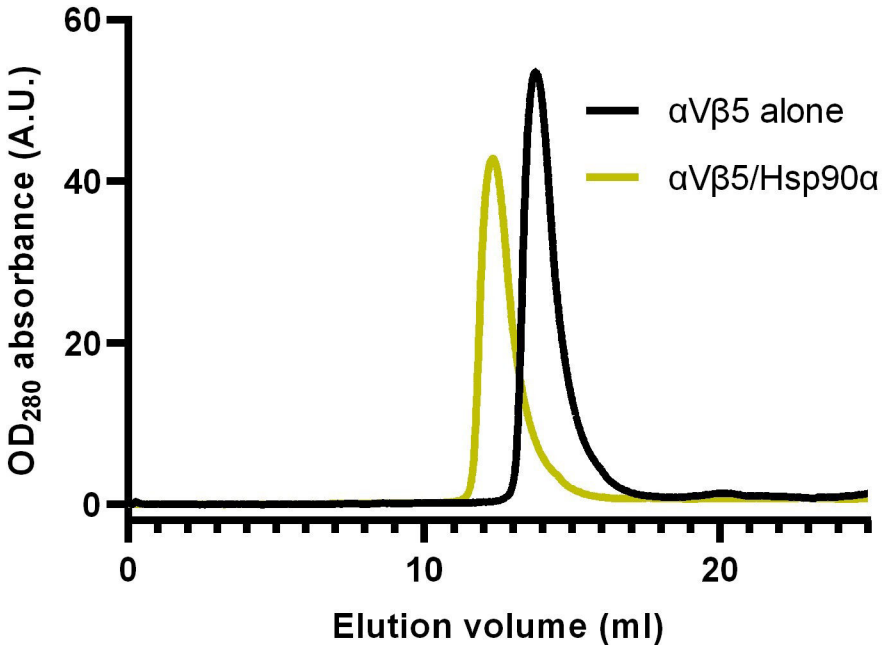

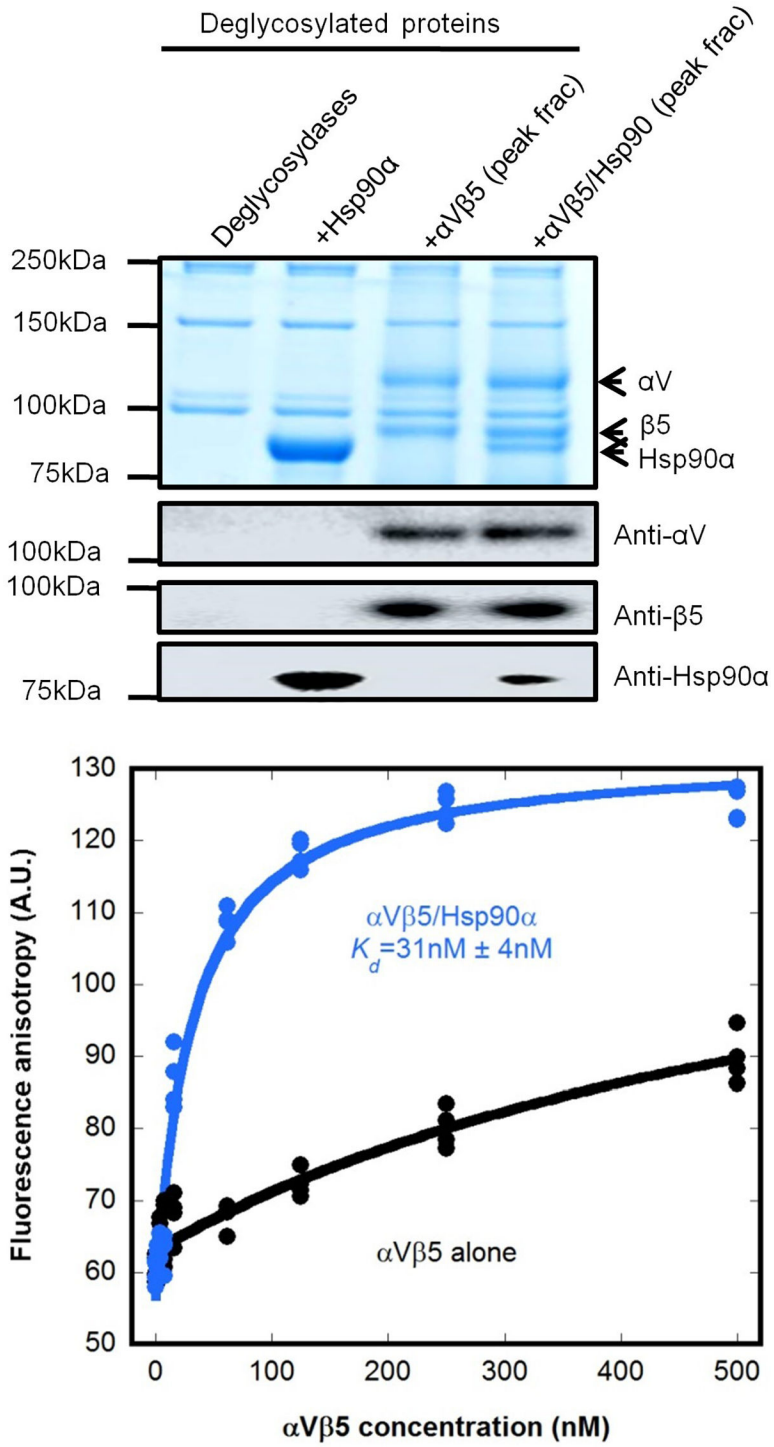

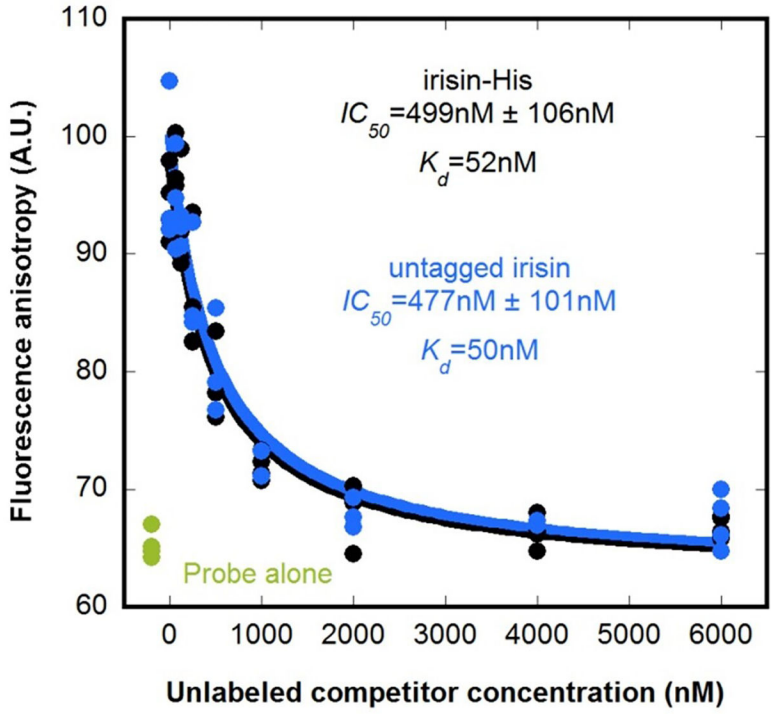

Figure 1: eHsp90α is required for irisin binding to integrin αVβ5.

(A) Schematic of the construct for recombinant human αVβ5 ectodomain protein production from mammalian cells. The domain boundaries are as follows: αV, 32–991; β5, 24–717. **(B)** and **(D)** Biolayerinferometry (BLI) measurement of binding of irisin to αVβ5. Purified irisin-His at the indicated concentration was infused over a sensor chip with immobilized clasped αVβ5 in the presence of 1 mM $MgCl_2$ and 1 mM $CaCl_2$. **(C)** Silver-stained SDS-polyacrylamide gel electrophoresis (SDS-PAGE) of affinity-purified αVβ5 fractions 7–20 collected following ion exchange. **(E)** A protein-elution profile of the indicated protein complexes from Superdex 200 increase 30/100 GL (optical density $(OD)_{280}$). **(F)** Coomassie-stained SDS-PAGE and western blot with the indicated antibodies of the deglycosylated recombinant human Hsp90α and peak fractions from (E). **(G)** Fluorescence anisotropy measurement of binding of αVβ5 and the αVβ5/Hsp90α complex to 50 nM A488-irisin-His in the presence of 1 mM $MgCl_2$ and 1 mM $CaCl_2$. **(H)** Fluorescence anisotropy competition assay for the αVβ5/Hsp90α complex binding by irisin: 50 nM A488-irisin-His and 125 nM αVβ5 were mixed with varying concentrations of unlabeled irisin or irisin-His, and anisotropy was recorded. Probe alone: 50 nM A488-irisin-His.

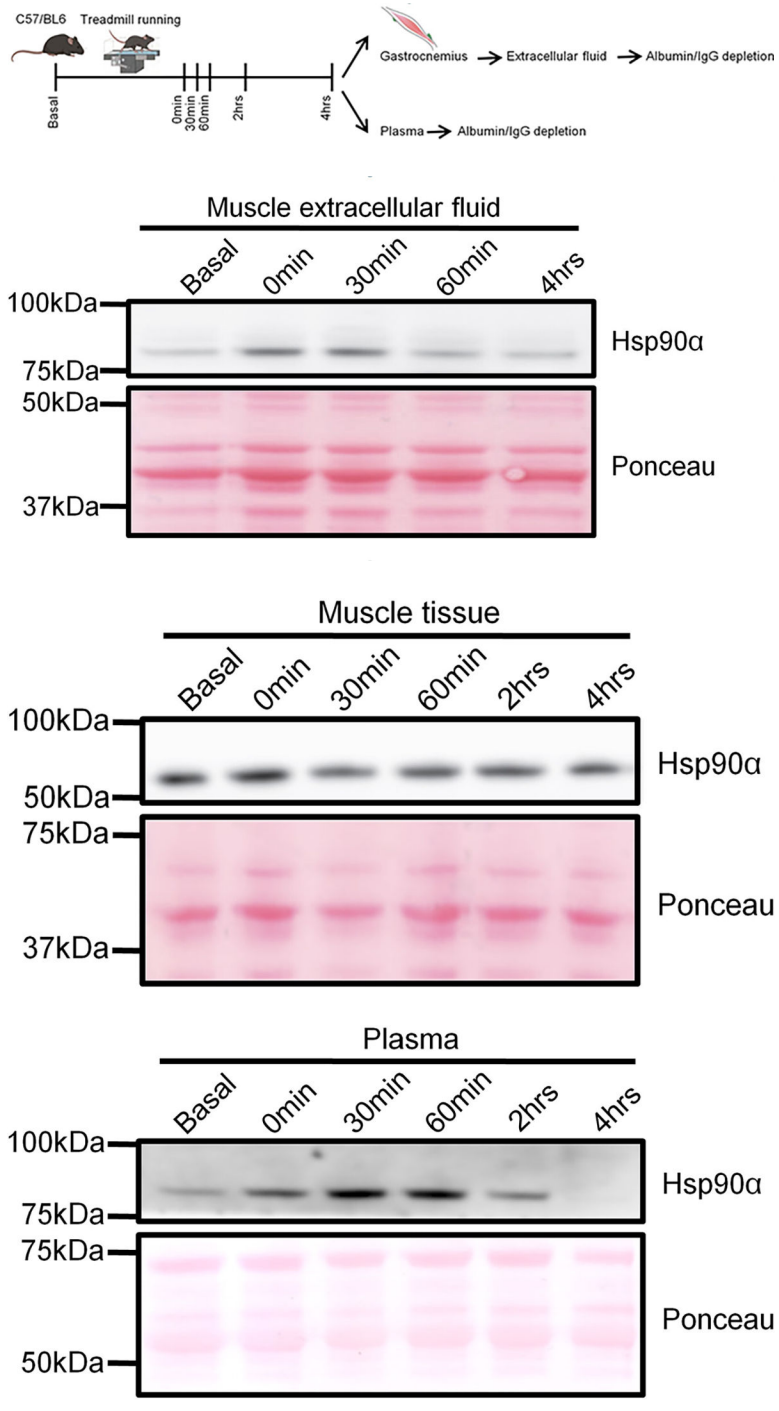

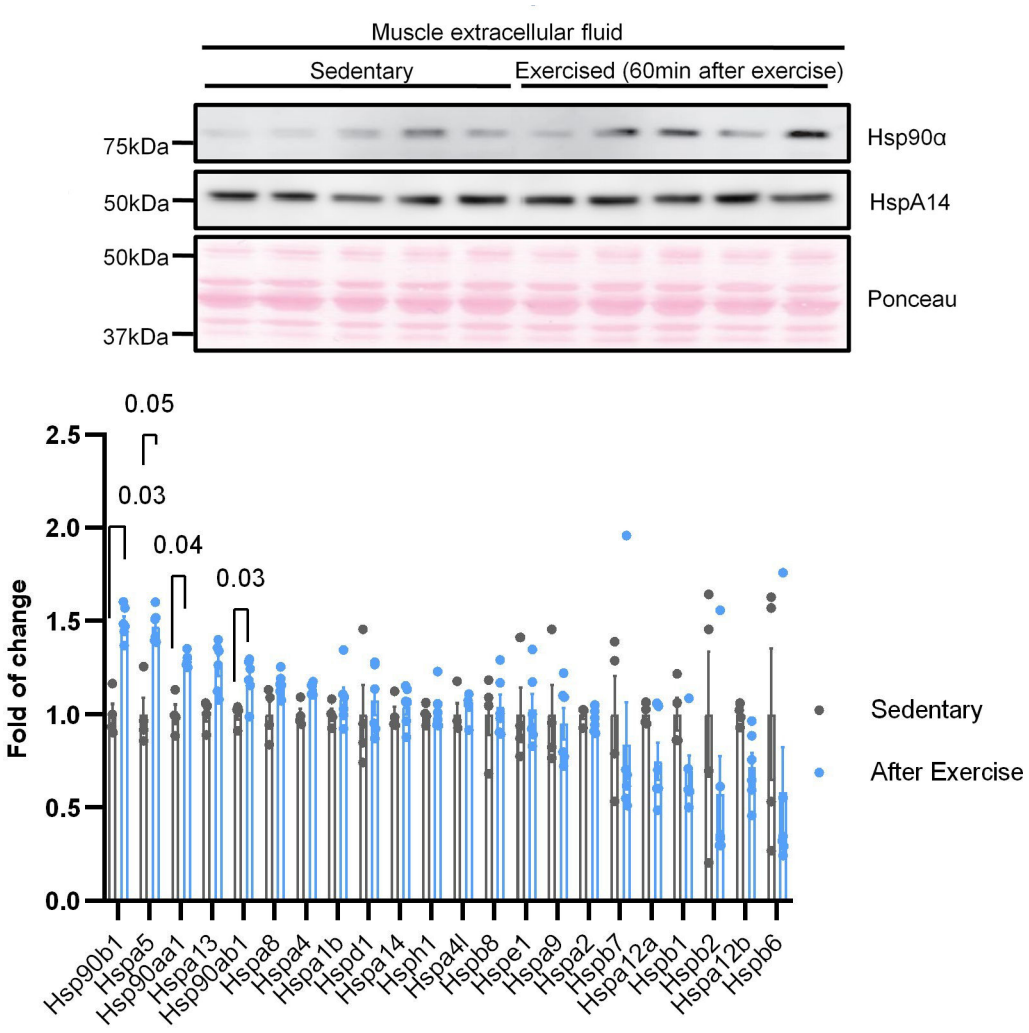

Figure 2: eHsp90αlevel is increased with exercise in muscle extracellular fluid and in plasma.

(A) Schematic of acute exercise and IF isolation procedure and processing. **(B)** Anti-Hsp90αwestern blot showing Hsp90α protein levels in IF samples taken from the mouse without acute exercise (basal), or from the mice rested for the indicated amounts of time after acute exercise. 10 μg of total IF protein was loaded for each sample as shown by Ponceau staining. **(C)** Anti-Hsp90α western blot showing Hsp90α protein levels in gastrocnemius muscle samples taken from the mouse without acute exercise (basal), or from the mice rested for the indicated amounts of time after acute exercise. 10 μg of total muscle protein was loaded for each sample as shown by Ponceau staining. **(D)** Anti-Hsp90αwestern blot showing Hsp90α protein levels in plasma samples taken from the same group of mice from (C). 10 μg of total plasma protein was loaded for each sample as shown by Ponceau staining. **(E)** Anti-Hsp90α and anti-HspA14 (control) western blot showing Hsp90α and HspA14 protein levels in plasma samples taken from five mice pre-exercise and post-exercise (1 hr). 10 μg of total plasma protein was loaded for each sample as shown by Ponceau staining. **(F)** Quantitative mass spectrometry showing the fold of changes of the indicated chaperone proteins identified in the IF samples from the exercised mice (1 hr post

acute exercise) compared to the sedentary group (significant if FDR q-value < 0.05).q-values of the significantly upregulated genes are indicated in the bar graph.

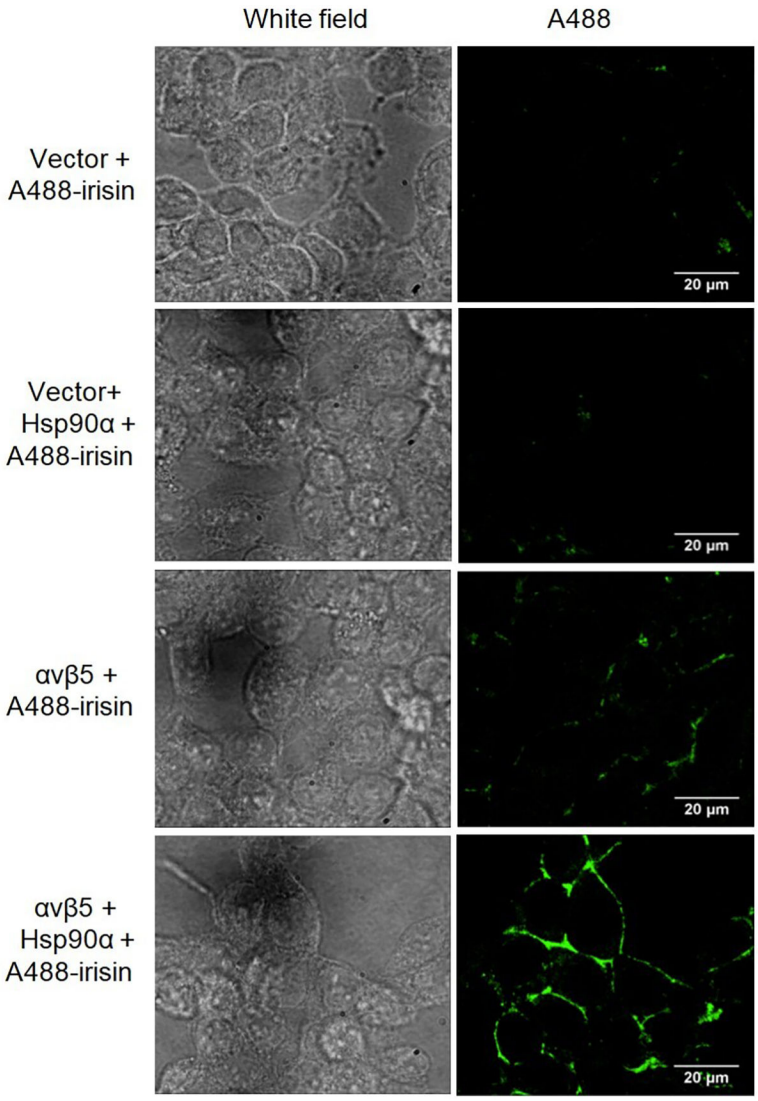

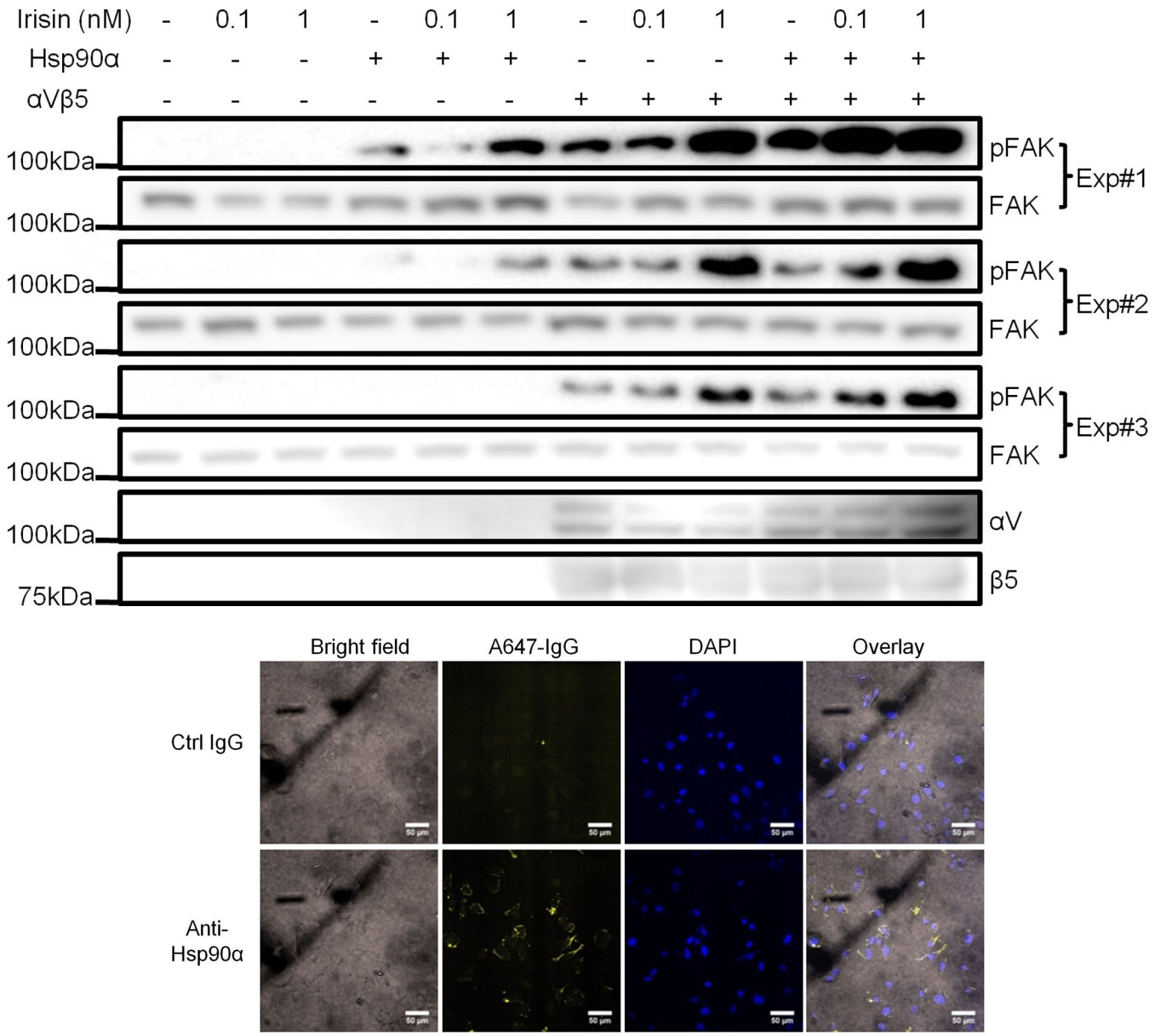

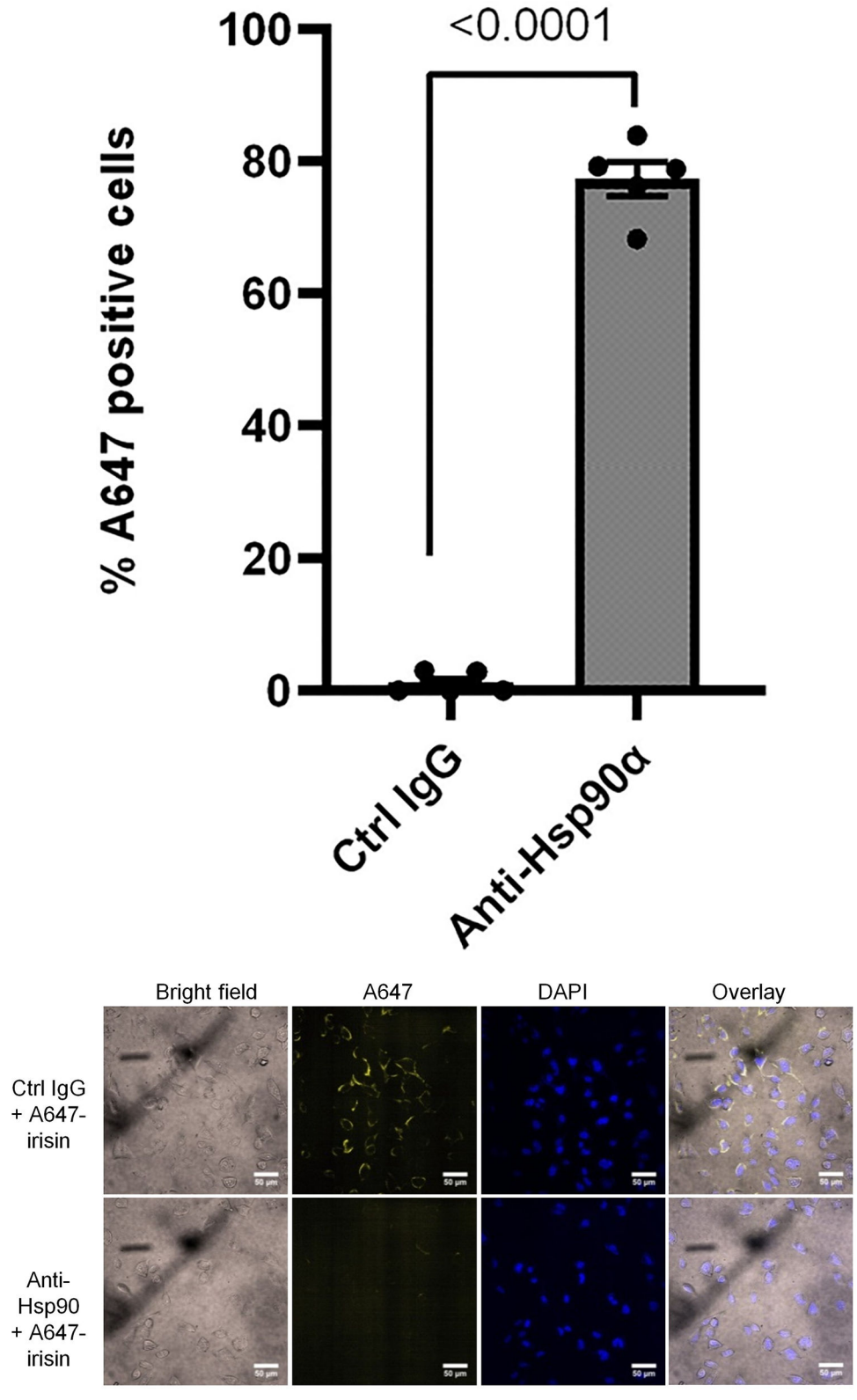

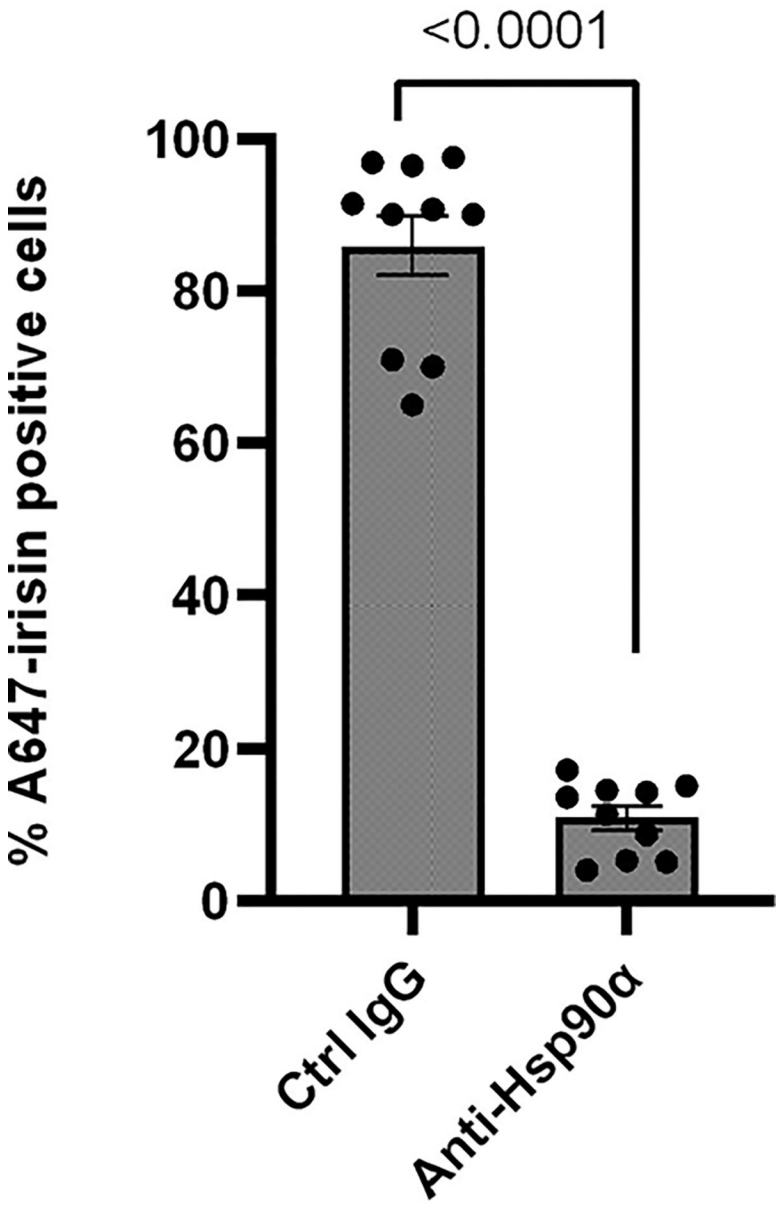

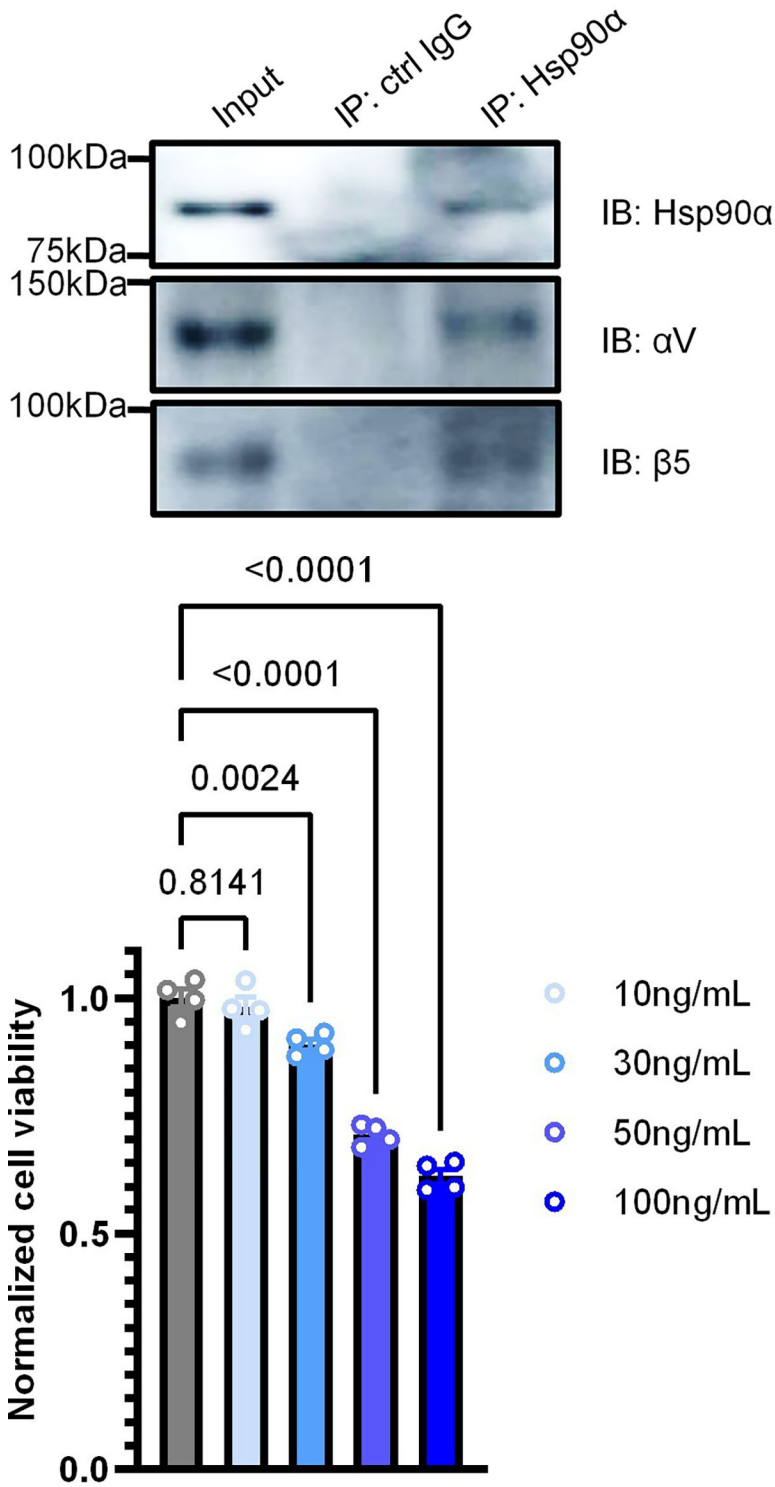

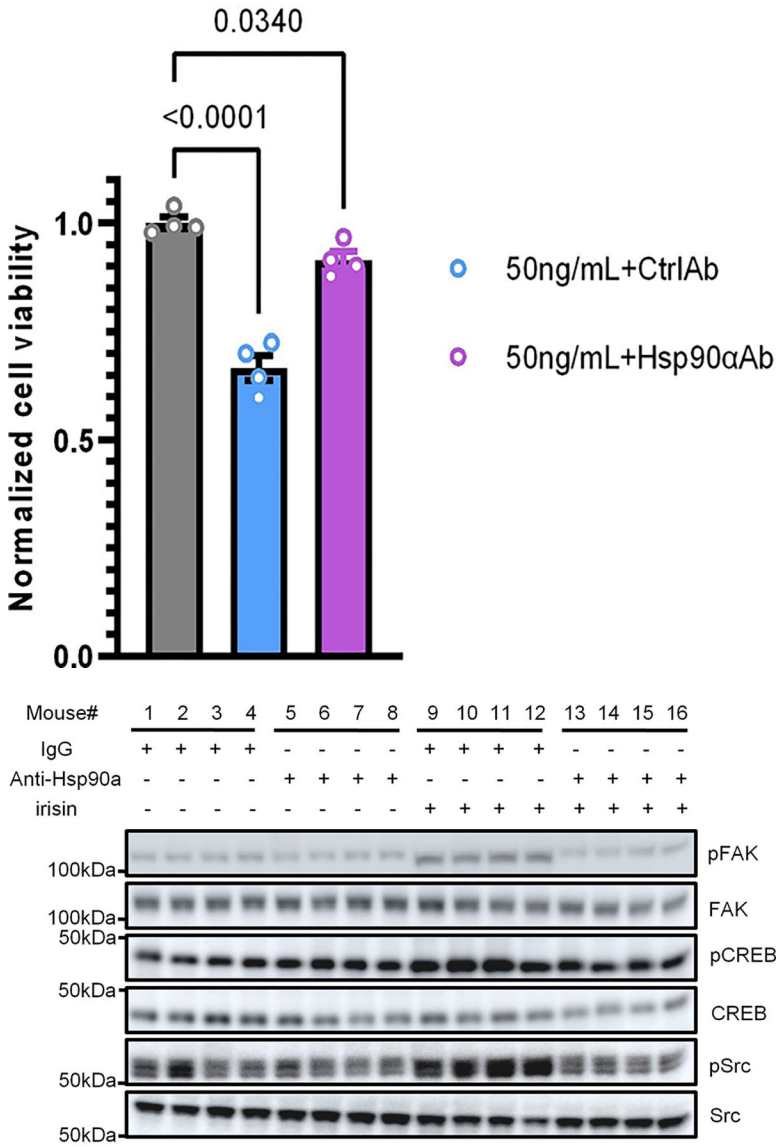

Figure 3: eHsp90α is required for optimal cellular actions of irisin.

(A) Fluorescence confocal images showing A488-irisin binding in HEK293T cells. HEK293T cells were either transiently transfected with control vector or full-length αV and β5 plasmids. 2 nM Hsp90α was used for 1 hr pretreatment, and 2 nM A488-irisin-His was subsequently used for 5 min treatment. Scale bar: 20 μm. **(B)** Anti-phosphorylated FAK (Y397) and anti-FAK western blots showing the levels of integrin signaling upon irisin and/or Hsp90α treatments. HEK293T cells were transfected and treated in the same way as (A), except for the addition of the shown amounts of unlabeled irisin-His (0.1 nM or 1 nM) and Hsp90α (1 nM). Anti-αV and anti-β5 antibodies were used to probe the levels of the ectopically expressed αV and β5. **(C)** Immunofluorescence confocal images showing cell surface Hsp90α in SK-Mel2 cells. Live cells were treated with either control IgG or anti-Hsp90α at 4°C. Scale bar: 50 μm. **(D)** Quantification of the percentage of SK-Mel2 cells expressing cell surface Hsp90α in (C) (significant if p-value < 0.05 by unpaired t-test). **(E)** Fluorescence confocal images showing A647-irisin binding in SK-Mel2

cells. Live cells were pretreated with either control IgG or anti-Hsp90α at 4°C for 1 hr followed by 2 nM A647-irisin-His treatment at room temperature for 5 min. Scale bar: 50 μm. **(F)** Quantification of the percentage of A647-positive cells in (E) (significant if p-value < 0.05 by unpaired t-test). **(G)** Co-immunoprecipitation assay of endogenous cell surface αV and β5 using SK-Mel2 cells. Endogenous cell surface Hsp90α was captured by anti-Hsp90α in live cells at 4°C. **(H)** Crystal violet assay showing does-dependent inhibition of the cell viability of SK-Mel2 upon irisin treatment. Grey bar: control treatment with PBS. Concentrations of irisin-His used for the treatments were indicated (one-way ANOVA). **(I)** Crystal violet assay showing the inhibition of irisin-mediated effect in SK-Mel2 cells by anti-Hsp90α or control antibody. Grey bar: control treatment with PBS. 50 ng/mL of irisin-His was used (one-way ANOVA). **(J)** Western blot of mouse inguinal fat tissue lysates using the indicated antibodies to probe integrin signaling. Mice were given anti-Hsp90α antibody or control IgG (500 μg/kg) subcutaneously 24 hrs before a bolus injection of recombinant irisin (5 mg/kg) directly into the inguinal fat pads. The mice were sacrificed and inguinal fat tissues were harvested 20 min after irisin injection.

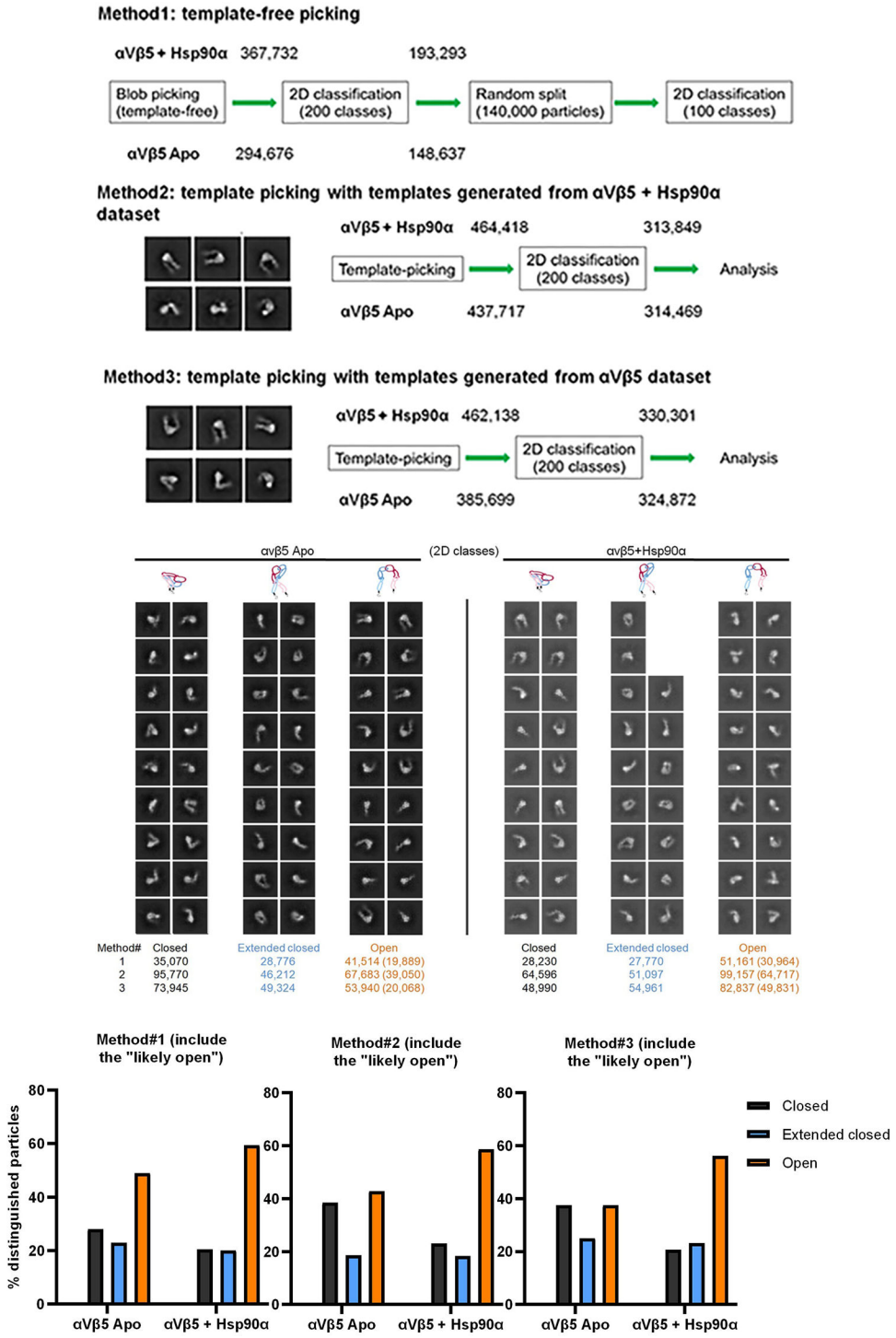

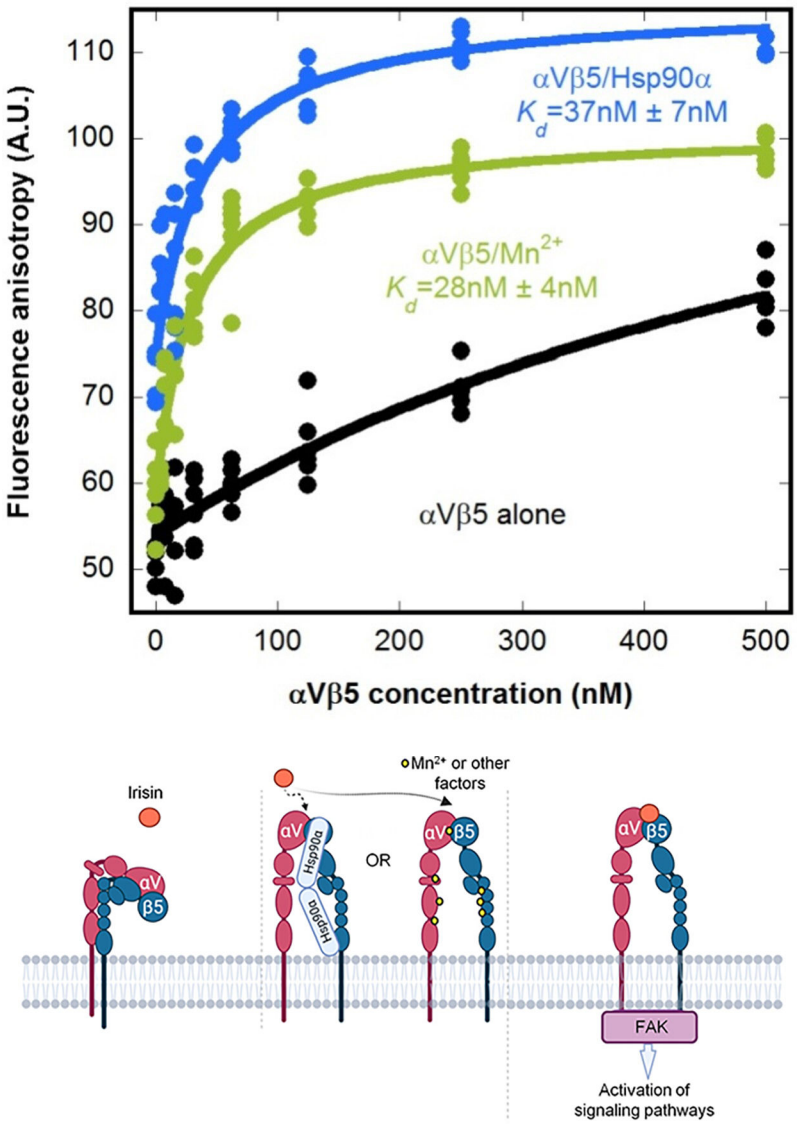

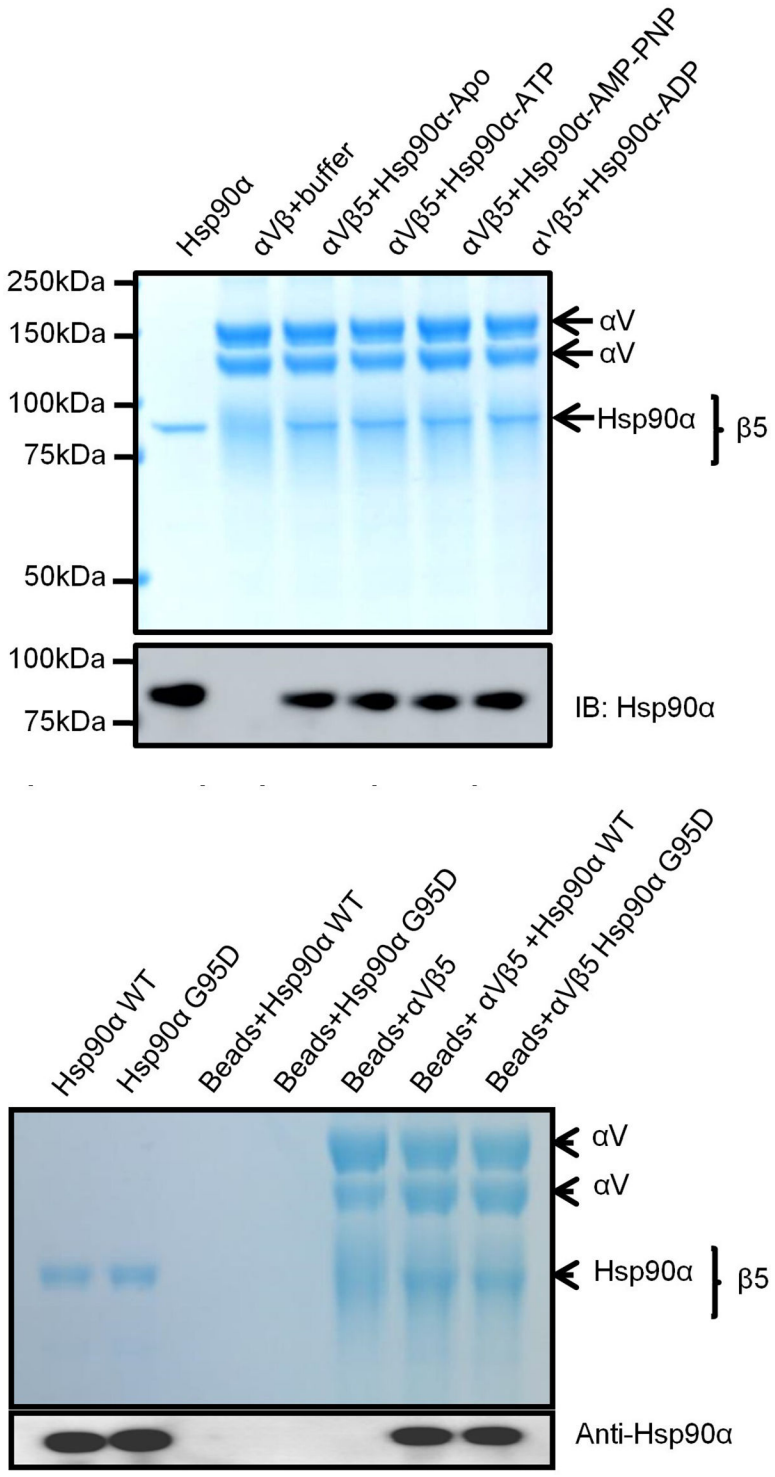

Figure 4: Hsp90α activates αVβ5 for irisin binding.

(A) Flow charts of the steps used in three different methods for analyzing αVβ5-Apo and αVβ5/Hsp90α cryo-EM samples. **(B)** 2D classes (generated by method 1) of αVβ5 particles in each of the three conformational states and the numbers (quantified by all three methods) of particles in each state. **(C)** Quantification of the percentage of distinguished

particles (“likely open” particles were not included) in each of the three conformational states. **(D)** Fluorescence anisotropy assay for A488-irisin binding by αVβ5, the αVβ5/Hsp90α complex in the presence of 1 mM $MgCl_2$ and 1 mM $CaCl_2$, or αVβ5 in the presence of 1 mM $MnCl_2$. 50 nM A488-irisin-His was used in the assay. **(E)** Cartoon diagram showing a two-step process of the irisin action through αVβ5. Irisin alone has low affinity for the closed-state αVβ5. Hsp90α, Mn^{2+} ion, or other possible factors, “opens” αVβ5, allowing for high-affinity irisin binding and effective signaling transduction through its integrin receptor. **(F) and (G)** TALON pull-downs performed using 1 μM bead-bound clasped and tagged αVβ5. These were mixed with 2 μM untagged Hsp90α without bound nucleotide (Hsp90α-Apo) or Hsp90α charged with the indicated nucleotides (F), or Hsp90α nonhydrolyzing mutant (G95D) (G), and bound samples were analyzed by Coomassie staining and anti-Hsp90α western blot.

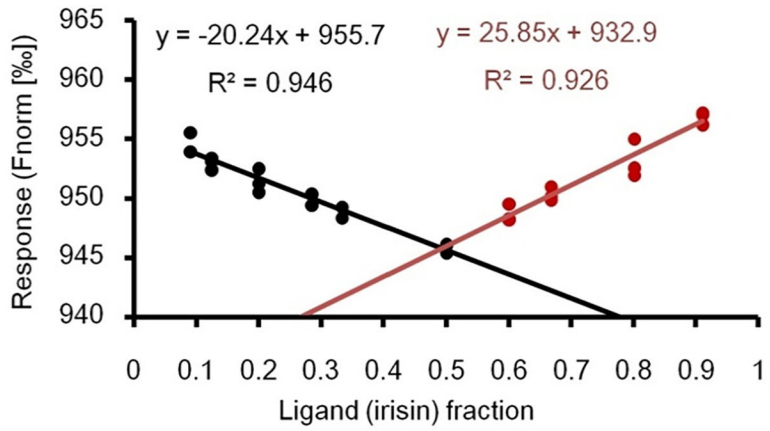

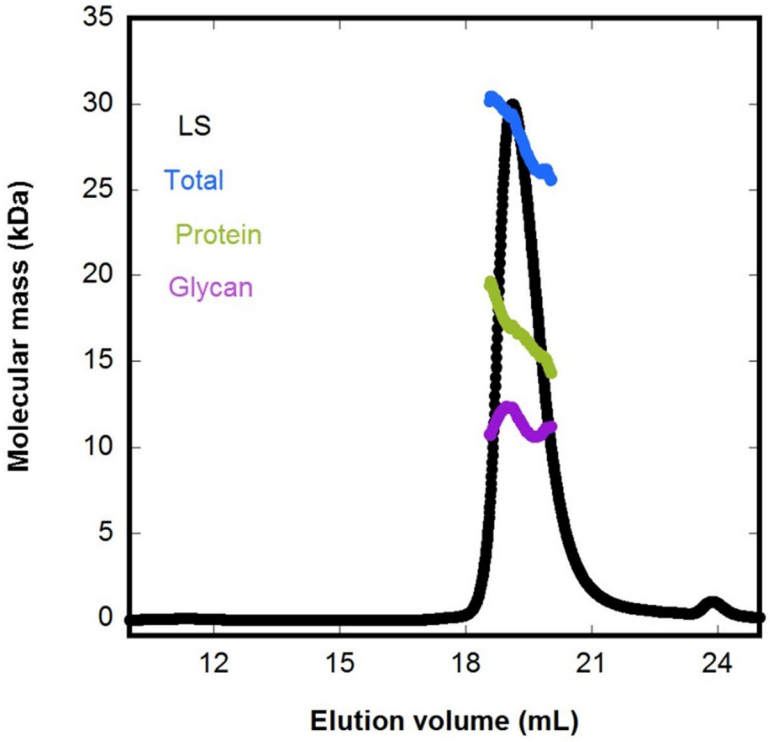

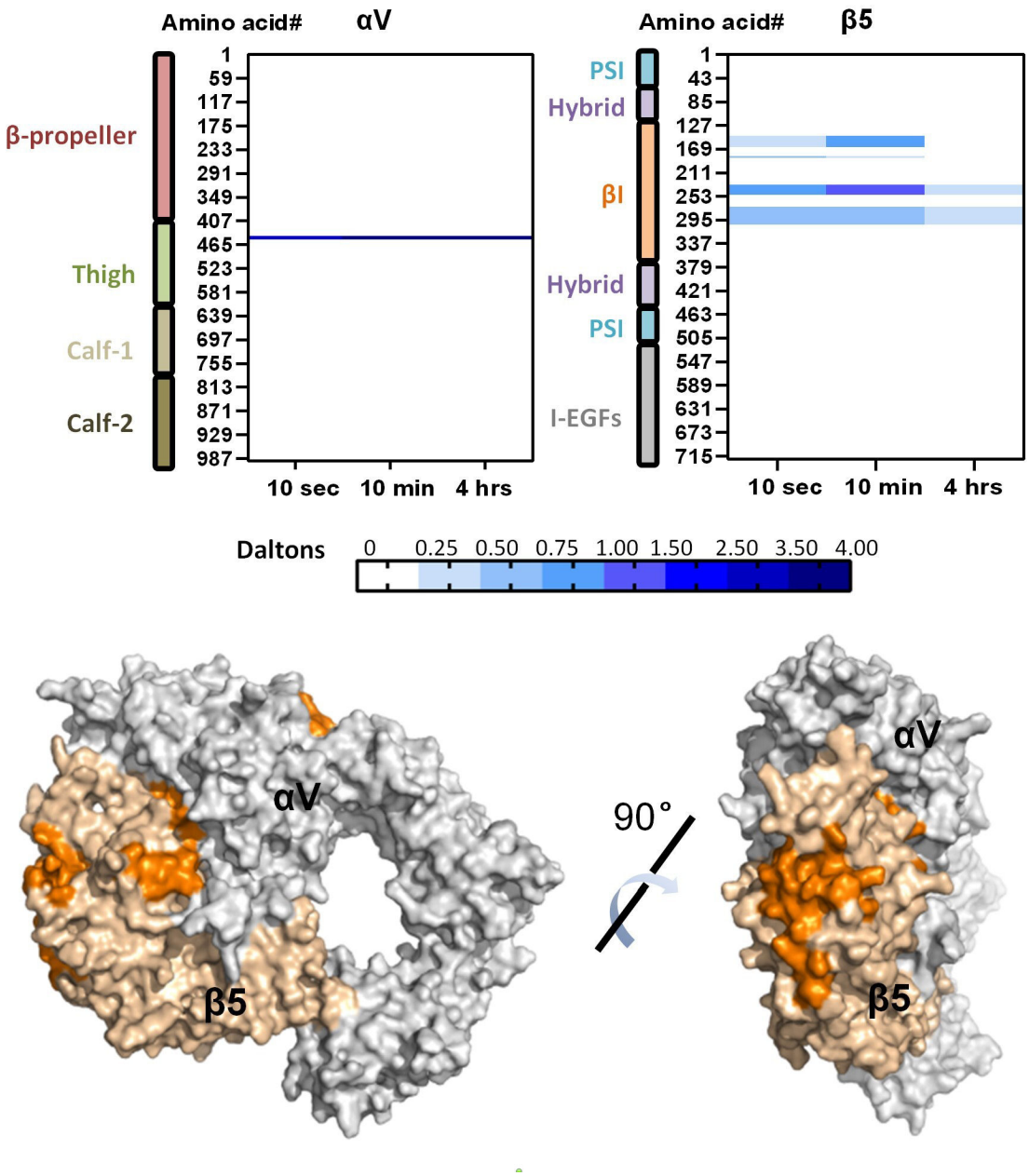

Figure 5: Biophysical characterization of the irisin/αVβ5 complex suggests an unconventional ligand-integrin interaction.

(A) MicroScale Thermophoresis (MST) measurement of the binding stoichiometry between A488-irisin-His and αVβ5 in the presence of 1 mM $MnCl_2$. MST responses were recorded at varying irisin: αVβ5 ratios with the total molar concentration of irisin plus αVβ5 constant (10 μM). **(B)** Size-exclusion chromatography and multiangle light scattering (SEC-MALS) determination of the absolute protein and glycan molecular mass of irisin-mam. 100 μg irisin-His was used in the assay. LS: light scattering; Total: total molecular mass of glycosylated irisin; Protein: molecular mass of the irisin protein; Glycan: molecular mass of the glycan. **(C)** Hydrogen/Deuterium exchange mass spectrometry (HDX-MS) mapping of the protected sites on αVβ5 in the irisin/αVβ5 complex. The measured relative deuterium

level of peptides in αVβ5-Apo at each deuteration time point was subtracted from the deuterium level of the corresponding peptide in the irisin/αVβ5 complex (D_{cplx} - D_{apo}), and the differences were colored according to the scale shown at the bottom. Peptides are shown from N- to C-terminus top to bottom, referring to the domain architecture on the left. The amount of time in deuterium is shown at the bottom. All deuterium uptake values used to generate these difference maps can be found in the Data S1. **(D)** Regions of αVβ5 protected from HDX in the irisin/αVβ5 complex (orange) on αVβ5 space filling structural model based on (C). αVβ5 structural model was generated from αVβ3 (PDB 1M1X) with β5 predicted by AlphaFold. αV subunit is in grey, and β5 subunit is in wheat.

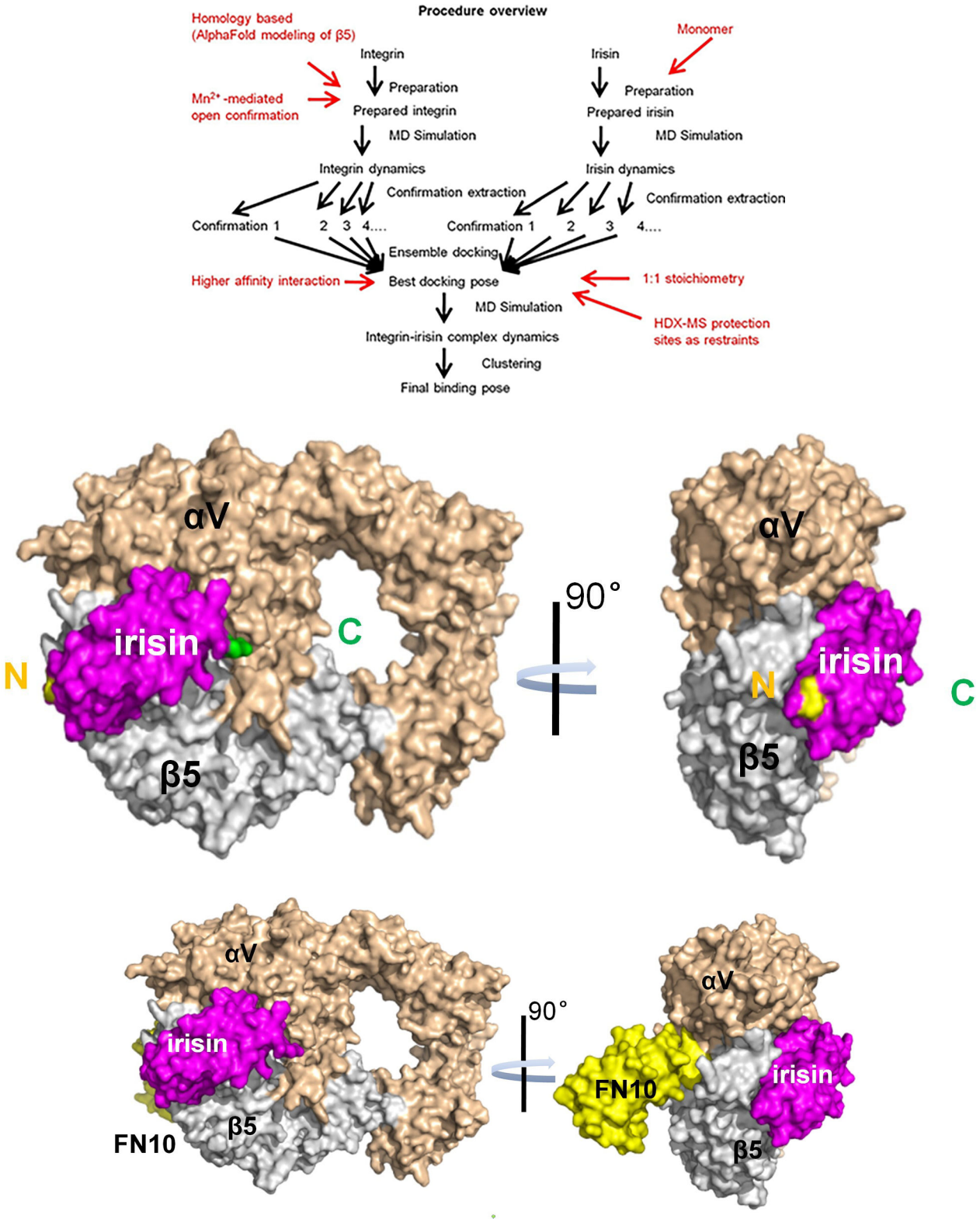

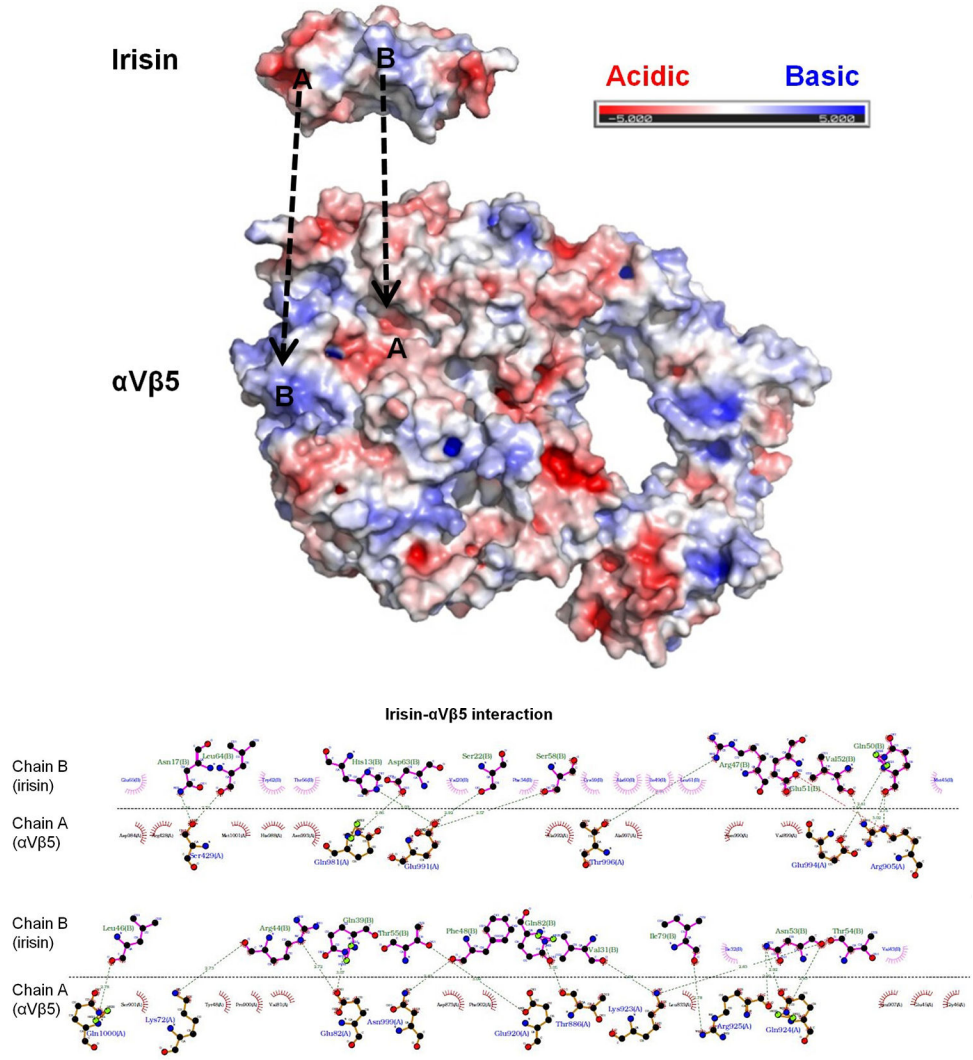

Figure 6: Docking model of the irisin/αVβ5 complex.

(A) Schematic of the irisin/αVβ5 complex modeling. Experimental results (red) were incorporated into the procedure in the indicated steps. **(B)** Space filling structural model of the irisin/αVβ5 complex. αV subunit is in beige, β5 subunit is in grey, and irisin is in magenta. The N- and C-terminus of irisin are highlighted in yellow and green, respectively. **(C)** Space filling structural model of the irisin/FN10/αVβ5 complex. αV subunit is in beige, β5 subunit is in grey, irisin is in magenta, and FN10 is in yellow. FN10-αVβ3 complex structure (PDB 4MMX) was used for fibronectin alignment to dock FN10 onto αVβ5. **(D)** Electrostatic potential surfaces of irisin (top) and αVβ5 (bottom). The surface charge distribution is displayed as blue for basic/positive, red for acidic/negative, and white for neutral. One acidic amino acid-rich region (A) and one basic amino acid-rich region (B) were shown on both irisin and αVβ5 at the interface. **(E)** Irisin-αVβ5 interactions in the irisin/αVβ5 complex model. Electrostatic interactions are in dashed lines between the atoms involved. The hydrophobic interactions are represented by arcs with spokes radiating towards the ligand atoms they contact, and the contacted atoms are shown with spokes radiating back.

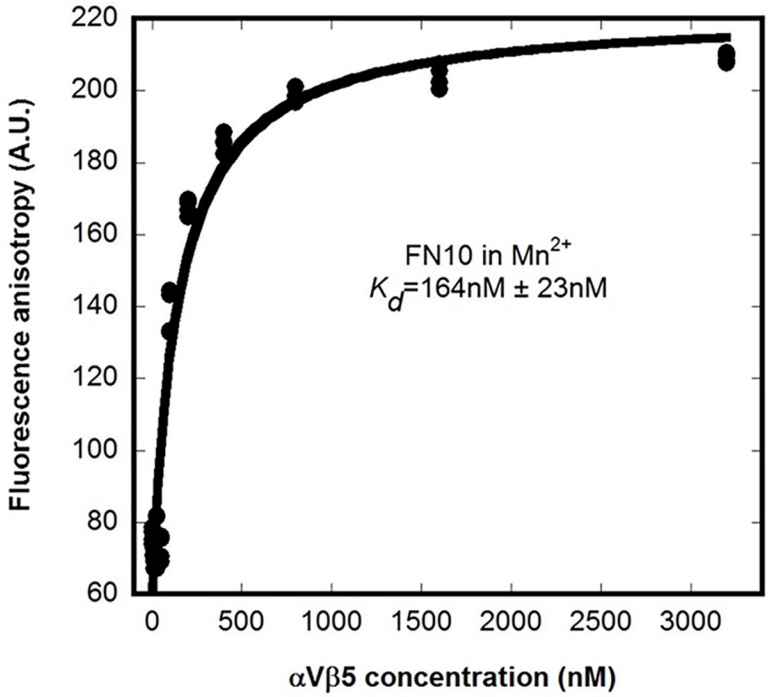

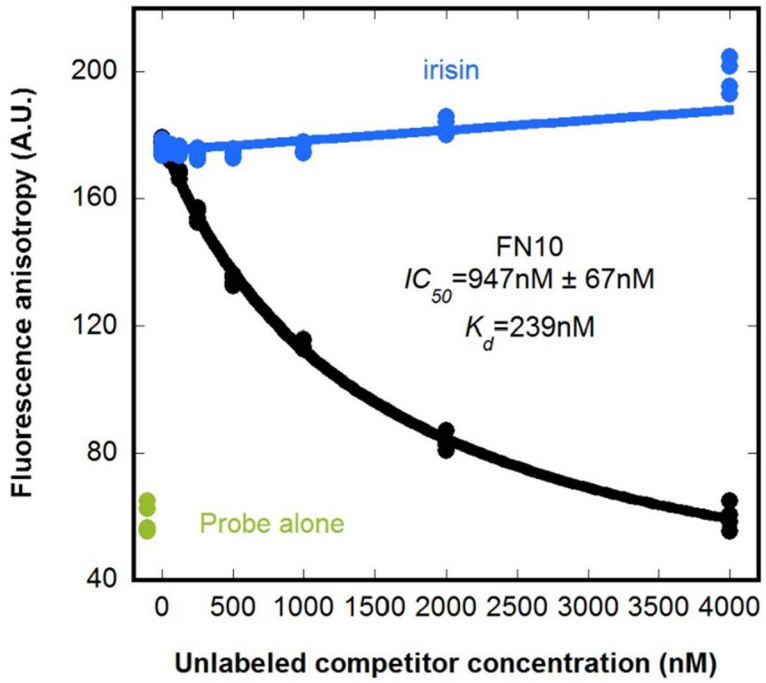

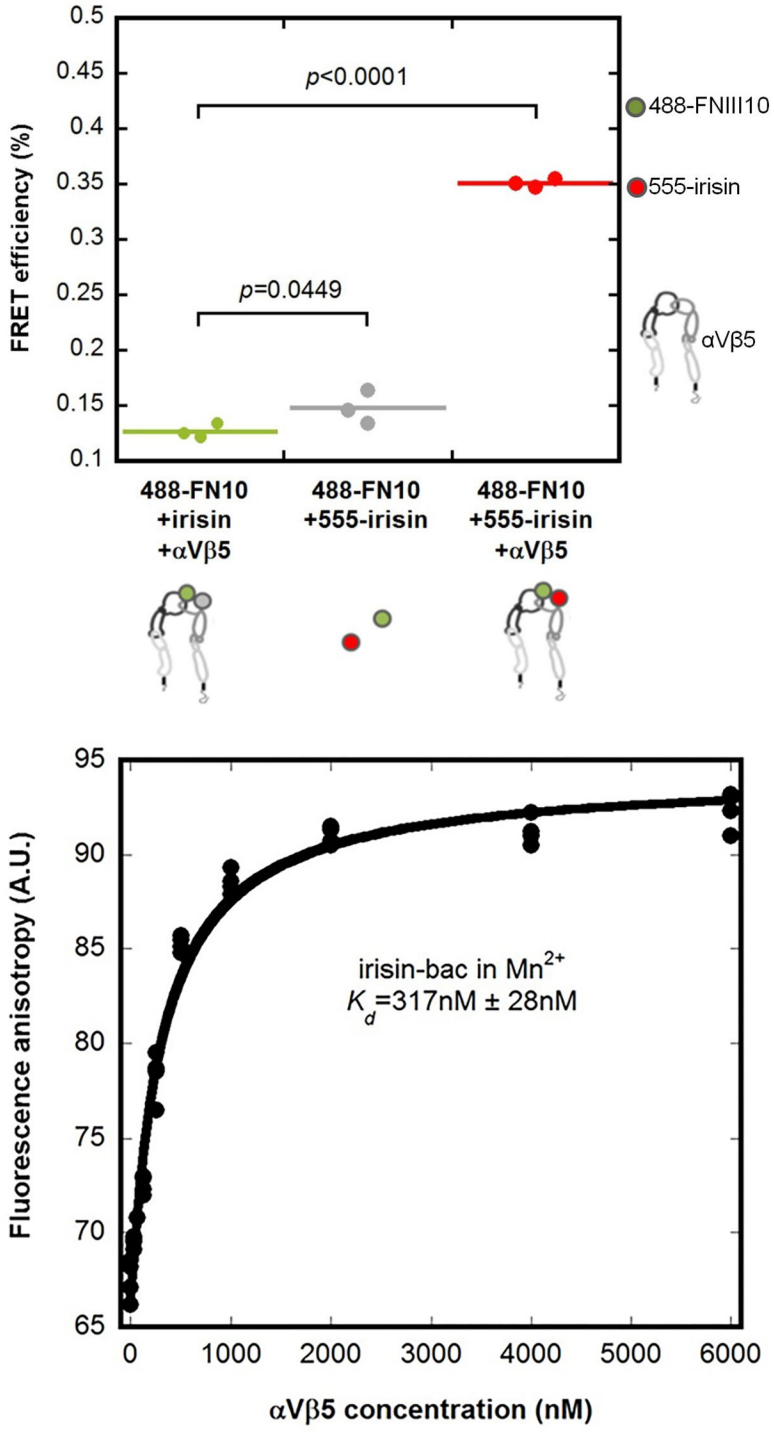

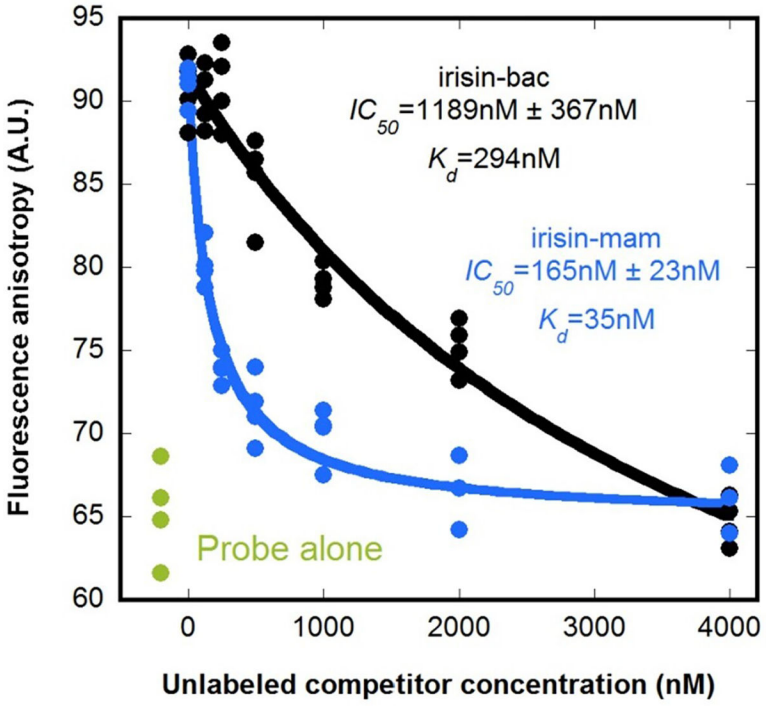

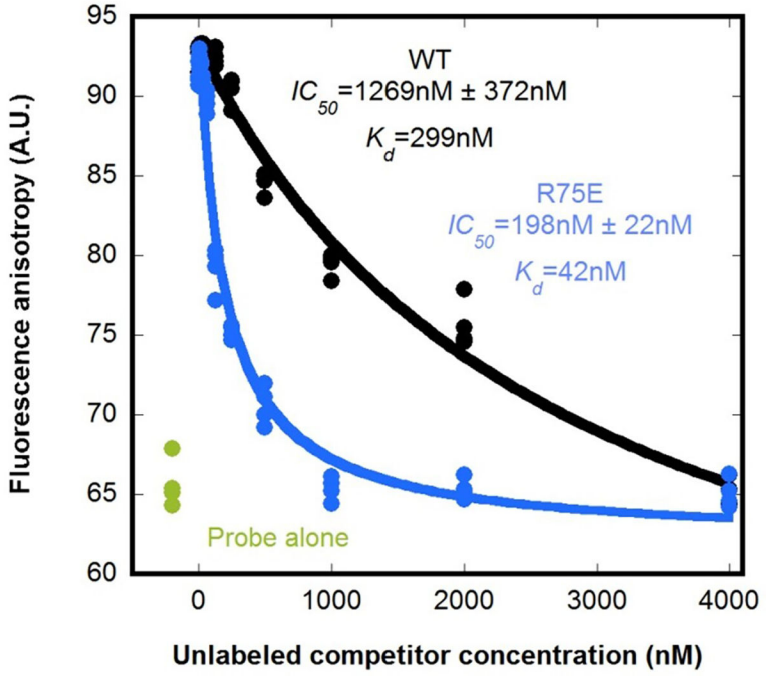

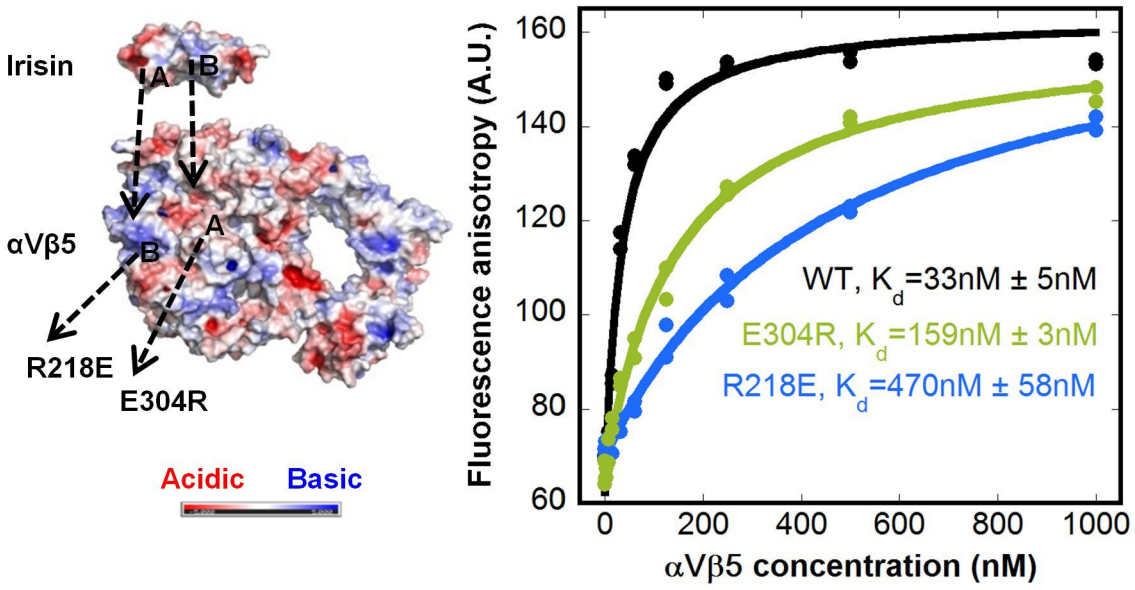

Figure 7: Validation of the irisin/αVβ5 complex model.

(A) Fluorescence anisotropy assay for A488-FN10 binding by αVβ5 in the presence of 1 mM $MnCl_2$. 50 nM A488-FN10 was used in the assay. **(B)** Fluorescence anisotropy competition assay for the αVβ5 binding by irisin or FN10: 50 nM A488-FN10 and 500 nM αVβ5 were mixed with varying concentrations of unlabeled irisin-His or FN10, and anisotropy was recorded. Probe alone: 50 nM A488-FN10. **(C)** Fluorescence resonance energy transfer (FRET) assay using 50 nM A488-FN10 and 50 nM unlabeled or A555 labeled irisin-His in the presence or absence of 500 nM αVβ5. FRET efficiency was calculated as the ratio of $F_{555}/(F_{488}+F_{555})$ where F_{555} is the acceptor emission and F_{488} is the donor emission (one-way ANOVA). **(D)** Fluorescence anisotropy assay for A488-irisin-bac binding by αVβ5 in the presence of 1 mM $MnCl_2$. **(E)** Fluorescence anisotropy competition assay for the αVβ5 binding by irisin-mam or irisin-bac: 50 nM A488-irisin-bac and 1000 nM αVβ5 were mixed with varying concentrations of unlabeled irisin-mam (irisin-His) or irisin-bac, and anisotropy was recorded. Probe alone: 50 nM A488-irisin-bac. **(F)** Fluorescence anisotropy competition assay for the αVβ5 binding by irisin-WT or irisin-R75E: 50 nM A488-irisin-WT and 1000 nM αVβ5 were mixed with varying concentrations of unlabeled irisin-WT or irisin-R75E, and anisotropy was recorded. Probe alone: 50 nM A488-irisin-WT. **(G)** Fluorescence anisotropy assay for A488-irisin binding by αVβ5 WT and indicated mutants (mutated residues are indicated in the space-filling model on the left) in the presence of 1 mM $MnCl_2$.

Key resources table

REAGENT or RESOURCE
Antibodies
Goat Polyclonal Anti-Mouse IgG (H+L) HRP Conjugate
Goat Polyclonal Anti-Rabbit IgG (H+L) HRP Conjugate
Rabbit Polyclonal Anti-phospho-FAK (Tyr397)
Rabbit Polyclonal Anti-FAK
Rabbit Monoclonal Anti-phospho-CREB (Ser133) (87G3)
Mouse Monoclonal Anti-CREB (86B10)
Rabbit Monoclonal Anti-Integrin αV (D2N5H)
Mouse IgG1 Isotype Control (Clone 11711)
Mouse Monoclonal Anti-Hsp90 (AC88)
Rabbit Polyclonal Anti-Hsp90α
Rabbit Monoclonal Anti- Integrin β5
Rabbit Polycloal Anti-6xHis tag
Rabbit Polyclonal Anti-Src
Rabbit Monoclonal Anti-phospho-Src (Tyr416) (D49G4)
Goat Anti-Mouse IgG (H+L) Cross-Adsorbed Secondary Antibody, Alexa Fluor 647
Bacterial and virus strains
T7-Express Competent *E. coli*
Biological samples
Chemicals, peptides, and recombinant proteins
10 His-tag irisin
Expi293F™ Expression Medium
Polyethylenumine, Linear, MW 25000

REAGENT or RESOURCE
DMEM media w/L-Glutamine, 4.5g/L glucose w/o Sodium pyruvate
RIPA buffer
FreeStyle293 Expression medium
TRIzol
Complete, Mini, EDTA-free (Protease Inhibitor)
PhosSTOP
Pierce™ Universal Nuclease for Cell Lysis
Lipofectamine™ 2000 Transfection Reagent
RNase Inhibitor
TMTpro 16plex Label Reagent Set
16% Paraformaldehyde
DAPI
Carbon Film 200 Mesh, Cu, 50/bx
C-flat™ Holey Carbon Grids
Critical commercial assays
R&D Systems Proteome Purify 2 Mouse Serum Protein Immunodepletion Resin
FX cloning system kit
ExpiFectamine™ 293 Transfection Kit
Ni Sepharose excel histidine-tagged protein purification resin
Mono Q™ 10/100 GL
HisPur™ Ni-NTA Superflow Agarose
Pierce™ Glutathione Agarose
Superdex 200 10/300 GL
Strep-Tactin Superflow High Capacity Resin
TALON Metal Affinity Resin
ToxinSensor™ Chromogenic LAL Endotoxin Assay Kit
ToxinEraser™ Endotoxin Removal Kit
Streptacidin Biosensors

REAGENT or RESOURCE
Protein Deglycosylation Mix II
cDNA Reverse-ATranscription Kit
Pierce™ Protein A Agarose
Standard Treated Capillaries
Pierce™ Detergent Compatible Bradford Assay Kit
RNeasy Mini Kit
RNase-Free DNase Set
GoTaq® qPCR and RT-qPCR Systems
Deposited data
HDX-MS dataset (related to Figure 5C and 5D)
Silver stained gel band mass spectrometry dataset
Unprocessed images
Experimental models: Cell lines
HEK293T
SK-Mel-2,
Expi293F
Experimental models: Organisms/strains
Mouse: C57BL/6J
Oligonucleotides
qPCR primer: UCP1 Forward: CACCTTCCCGCTGGACACT
qPCR primer: UCP1 Reverse: CCCTAGGACACCTTTATACCTAATGG
qPCR primer: Dio2 Forward: AATTATGCCTCGGAGAAGACCG
qPCR primer: Dio2 Reverse: T GGCAGTTGCCTAGTGAAAGGT
qPCR primer: Cidea Forward: TGACATTCATGGGATTGCAGAC
qPCR primer: Cidea Reverse: GGCCAGTTGTGATGACTAAGAC
qPCR primer: pGC1α Forward: CCCTGCCATTGTTAAGACC
qPCR primer: pGC1αReverse: TGCTGCTGTTCCTGTTTTC
qPCR primer: ALPL Forward: TCAACACCAATGTAGCCAAGA

REAGENT or RESOURCE
qPCR primer: ALPL Reverse: GTAGCTGGCCCTTAAGGATTC
qPCR primer: Cox8b Forward: GAACCATGAAGCCAACGACT
qPCR primer: Cox8b Reverse: GCGAAGTTCACAGTGGTTCC
qPCR primer: Rlpl0 Forward: GGAGTGACATCGTCTTTAAACCCC
qPCR primer: Rlpl0 Reverse: TCTGCTCCCACAATGAAGCA
g-Block dsDNA: Integrin αV (2627–2865bp)-Cyslinker-Acidic CC-2xstrep: ttgtctgccaagttgggagattagacagaggaaagagtgcaatcttgtacgtaaagtcattactgtggactgagacttttatgaataaagaaaatca
g-Block dsDNA: Integrin β5 (1850–2151bp)-Cyslinker-basic CC-8xHis-EcoR1: AGCCGGGGGCCTTTGGGGAGATGTGTGAGAAGTGCCCCACCTGCCCGGATGCATGCAGCACCAAGAGAGATTGCGTCGAGTGCCCGCTGCTCCACTCTGGGAAA
Primer: Cloning Integrin αV Forward: TTTTGGATCCGCCACCatggctt ttcc
Primer: Cloning Integrin β5 Forward: TTTTGGATCCGCCACCATG CCGCGTG
Primer: Cloning Integrin αV and Integrin β5 Reverse: ATTGGATTGGAAGTACAGGTTC
Primer: FX Cloning of Hsp90α Forward: atatatGCTCTTCtAGTcctgaggaaacccagacccaagaccaa
Primer: FX Cloning of Hsp90α Reverse: tatataGCTCTTCaTGCgtctacttcttccatgcgtgatgtgtc
Primer: FX Cloning of Hsp70 Forward: atatatGCTCTTCtAGTgcTaaagcTgcggcgatcggcatcgac
Primer: FX Cloning of Hsp70 Reverse: tatataGCTCTTCaTGCatctacctcctcaatggtggggcctga
g-Block dsDNA: Fibronectin 10th FNIII domain: ATATATGCTCTTCTAGTACTGTATCAGACGTGCCACGTGACTTAGAAGTCGTAGCAGCAACACCGACAAGTCTTTTGA
Primer: Site-directed Mutagenesis of Integrin β5 R218E mutant Forward: CCTCCTTTGGGTTCGAACATCTGCTGCCTCTCAC
Primer: Site-directed Mutagenesis of Integrin β5 R218E mutant Reverse: GTGAGAGGCAGCAGATGTTCGAACCCAAAGGAGG
Primer: Site-directed Mutagenesis of Integrin β5 E304R mutant Forward: GTGCCACCTGAACAGGGCCAACGAGTACACTG
Primer: Site-directed Mutagenesis of Integrin β5 E304R mutant Reverse: CAGTGTACTCGTTGGCCCTGTTCAGGTGGCAC
Primer: Site-directed Mutagenesis of Hsp90α G95D mutant Forward: GTGGATACTGGAATTGATATGACCAAGGCTGACTTG
Primer: Site-directed Mutagenesis of Hsp90α G95D mutant Reverse: CAAGTCAGCCTTGGTCATATCAATTCCAGTATCCAC
Recombinant DNA
cDNA ITGAV
cDNA ITGB5
cDNA HSP90AA1
cDNA HSPA1A
cDNA Irisin for Bacterial Expression
cDNA Irisin R75E for Bacterial Expression
Software and algorithms
ImageJ software
GraphPad Prism 9
KaleidaGraph Prism 4.5

REAGENT or RESOURCE
Biorender
cryoSPARC
ASTRA7
PLGS3.0.1
DynamX 3.0
Solution Builder
PDB-Tools
HADDOCK Web Server
Other
20 μm Nylon Mesh for EF Isolation
35 mm Dish | No. 1.5 Coverslip | 14 mm Glass Diameter | Uncoated